Advances in Nano Research, *Vol. 7 No. 2 (2019) 109-123*
DOI: https://doi.org/10.12989/anr.2019.7.2.109

Free vibration of an annular sandwich plate with CNTRC facesheets and FG porous cores using Ritz method

Mohsen Emdadi, Mehdi Mohammadimehr* and Borhan Rousta Navi

Department of Solid Mechanics, Faculty of Mechanical Engineering, University of Kashan, Kashan, P.O. Box 87317-53153, Iran

(*Received December 15, 2018, Revised March 2, 2019, Accepted March 30, 2019*)

Abstract. In this article, the free vibration analysis of annular sandwich plates with various functionally graded (FG) porous cores and carbon nanotubes reinforced composite (CNTRC) facesheets is investigated based on modified couple stress theory (MCST) and first order shear deformation theories (FSDT). The annular sandwich plate is composed of two face layers and a functionally graded porous core layer which contains different porosity distributions. Various approaches such as extended mixture rule (EMR), Eshelby-Mori-Tanaka (E-M-T), and Halpin-Tsai (H-T) are used to determine the effective material properties of microcomposite circular sandwich plate. The governing equations of motion are extracted by using Hamilton's principle and FSDT. A Ritz method has been utilized to calculate the natural frequency of an annular sandwich plate. The effects of material length scale parameters, boundary conditions, aspect and inner-outer radius ratios, FG porous distributions, pore compressibility and volume fractions of CNTs are considered. The results are obtained by Ritz solutions that can be served as benchmark data to validate their numerical and analytical methods in the future work and also in solid-state physics, materials science, and micro-electro-mechanical devices.

Keywords: free vibration analysis; circular annular sandwich plate; FG-porous core; CNTRC facesheets; EMR; EMT; HT approaches

1. Introduction

The porous materials, such as metal foams, have been made of two elements; one of which is solid (body) and the other element is either liquid or gas. Many researchers are interested to use these materials as advanced engineering materials (Ashby *et al.* 2000, Smith *et al.* 2012, Zhao 2012, Dukhan 2013, Betts 2012, Chen *et al.* 2016) in aerospace, civil constructions and automotive industry especially as a core of sandwich structures due to their excellent multi functionality offered by low specific weight, efficient capacity of energy dissipation, reduced thermal and electrical conductivity, and enhanced recyclability.

Sandwich structures have been usually made of three major parts: two thin facesheets layers that provide the in-plane and bending stiffness and a thick core sandwiched between facesheets that carries the transverse normal and shear loads. For these reasons, employing stiff facesheets such as carbon nanotubes (CNT) reinforced composite and low specific weight core such as porous materials (Mojahedin *et al.* 2016, Jasion and Magnucki 2013) is suggested. Wen (2012) presented an analytical solution for the deformation of a thick circular plate saturated by an incompressible fluid. Buckling analysis of porous beams with varying properties is described by Magnucki and Stasiewicz (2004). They used the shear deformation theory to determine the critical buckling load and also showed the effect of porosity on the strength and buckling load of the beam is investigated. Yahia *et al.* (2015) developed different higher order shear deformation plate theories for wave propagation in functionally graded plates. They investigated the effects of the volume fraction distributions and porosity volume fraction on wave propagation of functionally graded plate. Chen *et al.* (2015) studied the elastic buckling and static bending problems of shear deformable FG porous beams within the frame of the Timoshenko beam theory and considered two different non-uniform porosity distribution patterns and four types of boundary conditions. Magnucka-Blandzi (2009) discussed on dynamic stability of a metal foam circular plate with varying properties. The same author also obtained the critical buckling load for a rectangular plate made of foam with two layers of perfect material.

Experimental and theoretical studies showed that CNTs have extraordinary mechanical properties over carbon fibers to improve the characteristics (Zhang 2017a, b, Jalaei *et al.* 2018). The face sheets can be laminated composites (Ugale *et al.* 2015), functionally graded materials (Zhu *et al.* 2014 , Belkorissat *et al.* 2015, Zenkour 2005, Ahouel *et al.* 2016) or polymer matrix with CNTs reinforcements (Sun *et al.* 2005, Jia *et al.* 2011, Whitney 1972, Lei *et al.* 2015, Ahouel *et al.* 2016, Zhang *et al.* 2016a, b, c). Bellifa *et al.* (2017) developed a nonlocal zeroth-order shear deformation theory for nonlinear postbuckling of nanobeams. They considered the shear deformation effect in the axial displacement within the use of shear forces instead of rotational displacement like in existing shear deformation

*Corresponding author, Ph.D., Associate Professor,
E-mail: mmohammadimehr@kashanu.ac.ir

http://www.techno-press.org/?journal=journal=anr&subpage=5 ISSN: 2287-237X (Print), 2287-2388 (Online)

theories.

Mohammadimehr *et al*. (2014) performed biaxial buckling and bending analysis of smart nanocomposite plate reinforced by CNT using the extended mixture rule approach. Yin *et al*. (2010) considered the vibration analysis of micro nonclassical Kirchhoff plate based on the modified couple stress theory (MCST). They concluded that as the thickness to be comparable with the material length scale parameter, the MCST natural frequency is dependent on the size dependent effect. Karami *et al*. (2018) presented a variational approach for wave dispersion in anisotropic doubly-curved nanoshells based on a new nonlocal strain gradient higher order shell theory. The study of the doubly-curved nanoshell as a continuum model, a new size-dependent higher order shear deformation theory is introduced by them. Wang *et al*. (2011) took into account vibration and static analyses of rectangular Kirchhoff plate based on the strain gradient theory (SGT). They illustrated that the critical buckling load and natural frequency affected significantly using the size dependent effect. Wang and Shen (2012) presented nonlinear vibration and bending analyses of sandwich plates with carbon nanotube reinforced composite. They investigated the effects of nanotube volume fraction, core-to-face sheet thickness ratio, temperature change, foundation stiffness, and in-plane boundary conditions on the nonlinear vibration characteristics and nonlinear bending behaviors of sandwich plates with a functionally graded-carbon nanotube (FG-CNT) reinforced composite facesheets.

Many researchers established the effect of size dependent on the mechanical properties of structures at micro and nano scales. It has been illustrated that classical continuum mechanics cannot indicate the size influences at micro and nano scale structures. On the way to overcome this problem, many nonlocal theories that consider additional material constants, such as the nonlocal elasticity theory (Mohammadimehr and Rahmati 2013, Bounouara *et al*. 2016, Zemri *et al*. 2015), the strain gradient theory (SGT), modified couple stress theory (MCST) (Mohammadimehr *et al*. 2016a,d, 2017, Ke and Wang 2013), and modified strain gradient theory (MSGT) (Kong *et al*. 2009, Mohammadimehr *et al*. 2018a, Zeighampour and Beni 2014). Mohammadimehr *et al*. (2016b) investigated MSGT Reddy rectangular plate model for biaxial buckling and bending analysis of double-coupled piezoelectric polymeric nanocomposite reinforced by FG-SWCNT. Al-Basyouni *et al*. (2015) considered size dependent bending and vibration analyses of functionally graded microbeams based on MCST and neutral surface position.

Some investigations based on different plate theories (Mohammadimehr and Shahedi 2017, Zhang *et al*. 2016c, d) have been performed. Bourada *et al*. (2015) analyzed a new simple shear and normal deformations theory for functionally graded beams. They showed the effect of the inclusion of transverse normal strain on the deflections and stresses. Mohammadimehr and Salemi (2014) presented SGT for bending and buckling analysis of functionally graded (FG) Mindlin nanoplate. Bellifa *et al*. (2018) investigated bending and free vibration analyses of functionally graded plates using a simple shear deformation theory and the concept of the neutral surface position.

Ritz method, a proven approximation technique, (Lei *et al*. 2014, 2016a, b, Zhang *et al*. 2015a, b, c, d) which is a generalized Rayleigh method, has been used in computational analyses. Zhang and Xiao (2017) considered the mechanical behavior of laminated CNT-reinforced composite skew plates subjected to a dynamic load that they used the element-free IMLS-Ritz method to solve the problems. Also, some researchers worked about nano and micro composite, elastic foundation and various size dependent effects in the literature (Ghorbanpour Arani *et al*. 2011a, b, 2012, Mohammadimehr *et al*. 2010, 2016c, d, 2017). Vibration analysis of CNT-reinforced thick laminated composite plates based on Reddy's higher-order shear deformation theory is presented by Zhang and Selim (2017). They incorporated HSDT with one of the element-free approaches to show the influence of various CNT orientation angles, CNT volume fraction, plate aspect ratio and the number of plate's layers on the non- dimensional natural frequencies. Mohammadimehr and Mehrabi (2017 and 2018) presented stability and free vibration analyses of double-bonded micro composite sandwich cylindrical shells conveying fluid flow.

In the present work, free vibration analysis of annular sandwich plates with carbon nanotubes reinforced composite (CNTRC) facesheets and various FG porous cores using modified couple stress (MCST) and first order shear deformation theories (FSDT) and Ritz method is studied. The proposed porous core has been made of open-cell metal foam which the mechanical property is used to derive the relationship between coefficients of porosity and mass density. Two non-uniform FG porosity distributions and a uniform distribution have been considered in this research. The carbon nanotubes reinforced composite facesheets are modeled by various carbon nanotubes distributions. By using Hamilton's principle, the governing equations of motion are solved by the Ritz method for a microcomposite annular sandwich plate. The effects of material length scale parameters, boundary conditions, and aspect and inner-outer radius ratios on the natural frequency have been presented. Moreover, the noteworthy items are the consequence of FG porous distributions and pore compressibility using porous material as a core and also volume fraction of CNT in the EMR method and comparing of various CNTs approaches as a reinforcement of facesheet on the results.

2. Porosity distributions

Consider a micro annular sandwich plate with an outer radius R_b and inner radius R_a, and its $r-\theta$ polar coordinate system that is shown in Fig. 1. The total plate thickness is $h_t = h_c + 2h_f$, where h_c denotes the core thickness and h_f is the thickness of facesheets that are assumed to be perfectly bonded to the core material. The internal pores Mojahedin *et al*. (2016) in the core are uniform or non-uniform FG porosity distributions as also shown in Fig. 1. Young modulus $E(z)$, shear modulus $G(z)$, and mass density $\rho(z)$

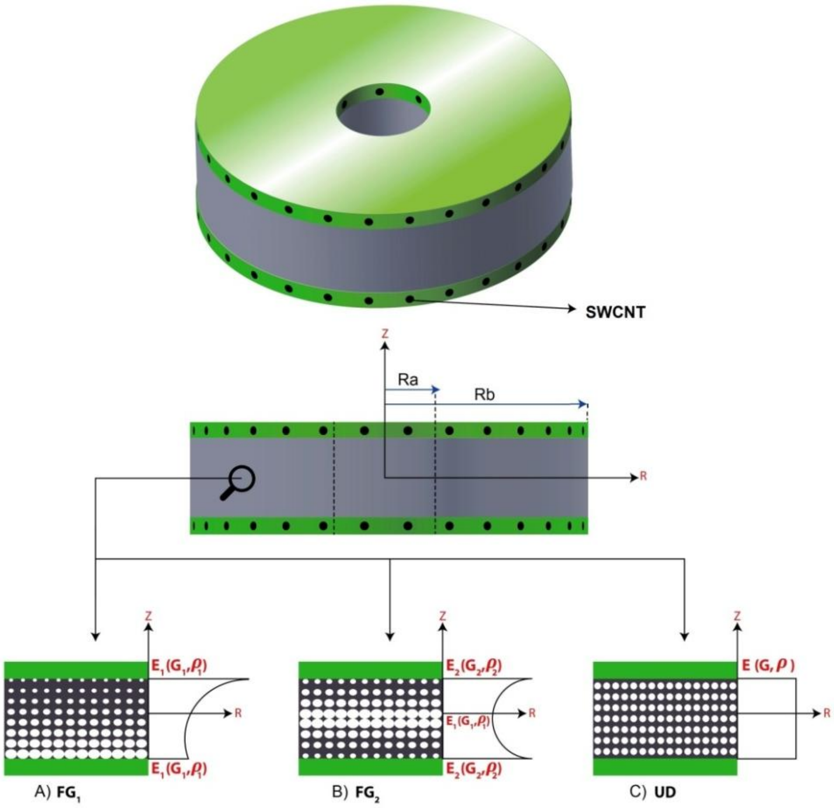

Fig. 1 A schematic diagram of the annular microcomposite sandwich plate with SWCNT reinforced composite facesheets and functionally graded porous cores.

are described in Eq. (1) for different kinds of distribution.

As it is observed in Fig. 1 that porosity distribution *A* is asymmetrical with continuous depression of material properties along thickness direction while porosity distribution *B* is symmetrical about r-axis with elastic moduli and mass density decreasing from top and bottom surfaces to the mid-plane. The porosity distribution *C* is uniform and without changing of depression in material properties along the thickness direction. The various porosity distributions are defined as follows (Mojahedin *et al*. 2016, Chen *et al*. 2016).

$$A,\begin{cases}E(z)=E_1\left[1-e_0\cos\left((\pi/2h_c)(z+h_c/2)\right)\right]\\ G(z)=G_1\left[1-e_0\cos\left((\pi/2h_c)(z+h_c/2)\right)\right]\\ \rho(z)=E_1\left[1-e_m\cos\left((\pi/2h_c)(z+h_c/2)\right)\right]\end{cases}$$

$$B,\begin{cases}E(z)=E_1\left[1-e_0\cos(\pi z/h_c)\right]\\ G(z)=G_1\left[1-e_0\cos(\pi z/h_c)\right]\\ \rho(z)=\rho_1\left[1-e_m\cos(\pi z/h_c)\right]\end{cases} \qquad (1)$$

$$C,\begin{cases}E(z)=E_1\left[1-e_0\varsigma\right]\\ G(z)=G_1\left[1-e_0\varsigma\right]\\ \rho(z)=\rho_1\sqrt{1-e_0\varsigma}\end{cases}$$

$$\varsigma=\frac{1}{e_0}-\frac{1}{e_0}\left(\frac{2}{\pi}\sqrt{1-e_0}-\frac{2}{\pi}+1\right)^2,\quad -h_c/2\le z\le h_c/2$$

where E_1, G_1 and ρ_1 are the corresponding maximum values of Young's modulus, shear modulus, and mass density for non-uniform porosity distributions, respectively. The material properties of the core are constant along the plate thickness for uniform porosity distribution and the coefficient ς is the equivalent mass of sandwich porous plates. e_0 and e_m are the coefficient of porosity and mass density, respectively, that can be defined as follows (Chen *et al*. 2016)

$$\begin{aligned}&e_0=1-\frac{E_2}{E_1}=1-\frac{G_2}{G_1},\ 0\le e_0\le 1\\ &e_m=1-\frac{\rho_2}{\rho_1},\ 0\le e_m\le 1\end{aligned} \qquad (2)$$

where E_2, G_2 and ρ_2 are the corresponding minimum values of Young's modulus, shear modulus, and mass density for non-uniform porosity distributions, respectively. The typical mechanical property of the open-cell metal foam and the relationship between e_0 and e_m are defined as follows (Chen v 2016)

$$\begin{aligned}&\frac{E_2}{E_1}=\left(\frac{\rho_2}{\rho_1}\right)^2\\ &e_m=1-\sqrt{1-e_0}\end{aligned} \qquad (3)$$

3. Various CNT distributions in the facesheets using different approaches

An annular sandwich plate is composed of three layers as shown in Fig. 1. It is assumed that the matrix is considered as an isotropic material and the CNT reinforced layers as top and bottom facesheets are made of various SWCNT models such as Eshelby-Mori-Tanaka (E-M-T), extended mixture rule (EMR), and Halpin-Tsai (H-T) in the thickness direction as follows:

3.1 The extended mixture rule approach

The effective material properties of the CNT reinforced matrix in extended mixture rule (EMR) approach are determined by the following equations (Mohammadimehr *et al*. 2018a)

$$
\begin{aligned}
&E_{11} = \eta_1 V_{CNT} E_{11}^{CNT} + V_m E_m \\
&\frac{\eta_2}{E_{22}} = \frac{V_{CNT}}{E_{22}^{CNT}} + \frac{V_m}{E_m} \\
&\frac{\eta_3}{G_{12}} = \frac{V_{CNT}}{G_{12}^{CNT}} + \frac{V_m}{G_m} \\
&\rho = \rho_{CNT} V_{CNT} + \rho_m V_m
\end{aligned}
\tag{4}
$$

where η_i (i = 1, 2, 3) denotes force transformation between SWCNTs and polymeric matrix and E_{11}, E_{22} and G_{12} are Young's moduli and the shear modulus of the CNT, and V_{CNT} and V_m are the volume fraction of the CNT and the matrix, respectively.

3.2 Eshelby-Mori-Tanaka approach

The other approach for estimation of material properties of the CNT fiber is Eshelby-Mori-Tanaka (E-M-T) approach that fiber is uniformly distributed in the isotropic matrix. The stiffness coefficients are written as follows (Ghorbanpour Arani *et al*. 2016)

$$
\begin{aligned}
Q_{11} &= \frac{E_m c_m (1+V_f - V_m \upsilon_m) + 2V_m V_f (k_f n_f - l_f^2)(1+\upsilon_m)^2 (1-2\upsilon_m)}{(1+\upsilon_m)\left\{2V_m k_f (1-\upsilon_m - 2\upsilon_m^2) + E_m (1+V_f - 2\upsilon_m)\right\}} \\
&+ \frac{E_m \left[2V_m^2 k_f (1-\upsilon_m) + V_f n_f (1-2\upsilon_m + V_f) - 4V_m l_f \upsilon_m\right]}{2V_m k_f (1-\upsilon_m - 2\upsilon_m^2) + E_m (1+V_f - 2\upsilon_m)} \\
Q_{22} &= \frac{E_m \left\{E_m V_m + 2k_f (1+\upsilon_m)\left[1+V_f (1-2\upsilon_m)\right]\right\}}{2(1+\upsilon_m)\left[E_m (1+V_f - 2\upsilon_m) + 2V_m k_f (1-\upsilon_m - 2\upsilon_m^2)\right]} \\
&+ \frac{E_m \left[E_m V_m + 2m_f (3+V_f - 4\upsilon_m)(1+\upsilon_m)\right]}{2(1+\upsilon_m)\left\{E_m \left[V_m + 4V_f (1-\upsilon_m)\right] + 2m_f V_m (3+V_f - 4\upsilon_m^2)\right\}}
\end{aligned}
\tag{5}
$$

$$
\begin{aligned}
Q_{12} &= \frac{E_m \left\{V_m \upsilon_m \left[E_m + 2k_f (1+\upsilon_m)\right] + 2V_f l_f (1-\upsilon_m^2)\right\}}{(1+\upsilon_m)\left[2V_m k_f (1-\upsilon_m - 2\upsilon_m^2) + E_m (1+V_f - 2\upsilon_m)\right]} \\
Q_{66} &= \frac{E_m \left[E_m V_m + 2(1+V_f) p_f (1+\upsilon_m)\right]}{2(1+\upsilon_m)\left[E_m (1+V_f) + 2V_m p_f (1+\upsilon_m)\right]}
\end{aligned}
\tag{5}
$$

where v_m is the Poisson's ratio of the matrix and k_f, n_f, m_f and p_f are the Hill's elastic moduli for CNTs.

3.3 Halpin-Tsai approach

Material properties of the circular sandwich facesheets in Halpin-Tsai (H-T) are defined as follows

$$E_1 = V_f E_f + V_m E_m \tag{6}$$

where V_f, V_m, E_f, and E_m are fiber and matrix volume fraction and moduli, respectively and the transverse modulus can be written as follows (Halpin and Kardos 1976)

$$\frac{E_2}{E_m} = \frac{1+\chi \eta_1 V_f}{1-\eta_1 V_f} \tag{7}$$

where χ = 2 is considered for the best state and η_1 is shown as the following form

$$\eta_1 = \frac{\frac{E_f}{E_m} - 1}{\frac{E_f}{E_m} + \chi} \tag{8}$$

The shear modulus, η_2 and χ = 1 for the best state are defined as follows

$$\frac{G_{12}}{G_m} = \frac{1+\chi \eta_2 V_f}{1-\eta_2 V_f} \tag{9}$$

$$\eta_2 = \frac{\frac{G_f}{G_m} - 1}{\frac{G_f}{G_m} + \chi} \tag{10}$$

where G_f and G_m are fiber and matrix moduli, respectively.

The volumes fractions are related by $V_{CNT} + V_m = 1$. The facesheets are supposed to be reinforced with CNTs and the volume fraction V_{CNT} for the top facesheet can be defined as (Mohammadimehr *et al*. 2018a)

$$V_{CNT} = 2\left(\frac{t_1 - z}{t_1 - t_0}\right) \overset{*}{V}_{CNT} \tag{11}$$

and for the bottom facesheet as follows

$$V_{CNT} = 2\left(\frac{z - t_2}{t_3 - t_2}\right) \overset{*}{V}_{CNT} \tag{12}$$

where

$$\overset{*}{V}_{CNT} = \frac{w_{CNT}}{w_{CNT} + \left(\frac{\rho_{CNT}}{\rho_m}\right)(1 - w_{CNT})} \tag{13}$$

where w_{CNT} is the mass fraction of the nanotubes. ρ_{CNT} and ρ_m are the mass densities of carbon nanotube and the matrix, respectively.

4. The theoretical formulation of a circular sandwich plate

According to the first order shear deformation theory (FSDT), the displacement fields for the micro composite sandwich plate is used as follows

$$\begin{aligned} u(r,\theta,z,t) &= u_0^o(r,\theta,t) + f(z)\alpha^o(r,\theta,t) \\ v(r,\theta,z,t) &= v_0^o(r,\theta,t) + f(z)\beta^o(r,\theta,t) \\ w(r,\theta,z,t) &= w_0^o(r,\theta,t) \end{aligned} \quad (14)$$

where u_0^o and v_0^o denote in-plane displacements on mid-plane in r and z directions, respectively and w_0^o is the transverse displacement of the plate. α^o and β^o are the rotation of the middle surface about r and θ at $z = 0$ and $f(z) = z$.

Strain–displacement relations according to first order shear deformation theory (FSDT) can be expressed as follows

$$\begin{aligned} \varepsilon_{rr}^o &= \frac{\partial u_0^o}{\partial r} + f(z)\frac{\partial \alpha^o}{\partial r} \\ \varepsilon_{\theta\theta}^o &= \frac{1}{r}\left(u_0^o + f(z)\alpha^o\right) \\ \varepsilon_{r\theta}^o &= -\frac{1}{2r}\left(v_0^o + f(z)\beta\right)^o + \frac{1}{2}\left(\frac{\partial v_0^o}{\partial r} + f(z)\frac{\partial \beta^o}{\partial r}\right) \\ \varepsilon_{rz}^o &= \frac{1}{2}\left(\frac{\partial f(z)}{\partial z}\alpha^o + \frac{\partial w_0^o}{\partial r}\right), \varepsilon_{\theta z}^o = \frac{1}{2}\left(\frac{\partial f(z)}{\partial z}\beta^o\right) \end{aligned} \quad (15)$$

Using Hook's law, the constitutive equations for the microcomposite annular sandwich plate can be stated as follows

$$\begin{Bmatrix} \sigma_{rr}^o \\ \sigma_{\theta\theta}^o \\ \sigma_{r\theta}^o \\ \sigma_{z\theta}^o \\ \sigma_{zr}^o \end{Bmatrix} = \begin{bmatrix} Q_{11}^o & Q_{12}^o & 0 & 0 & 0 \\ Q_{12}^o & Q_{22}^o & 0 & 0 & 0 \\ 0 & 0 & Q_{66}^o & 0 & 0 \\ 0 & 0 & 0 & Q_{44}^o & 0 \\ 0 & 0 & 0 & 0 & Q_{55}^o \end{bmatrix} \begin{Bmatrix} \varepsilon_{rr}^o \\ \varepsilon_{\theta\theta}^o \\ \varepsilon_{r\theta}^o \\ \varepsilon_{z\theta}^o \\ \varepsilon_{zr}^o \end{Bmatrix} \quad (16)$$

where Q_{ij}^o, σ_{ij}^o and ε_{ij}^o are the stiffness coefficient matrix, stress and strain components, respectively. Upper index, $o(t, c, b)$ denotes the layers of microcomposite sandwich (top, core, bottom) and Q_{ij}^o is defined as follows

$$\begin{aligned} &Q_{11}^o = \frac{E_{11}^0}{1-\nu_{12}^0\nu_{21}^0}, Q_{22}^o = \frac{E_{22}^0}{1-\nu_{12}^0\nu_{21}^0}, Q_{12}^o = \frac{\nu_{21}^0 E_{11}^0}{1-\nu_{12}^0\nu_{21}^0}, \\ &Q_{44}^o = k_s G_{23}^0, Q_{55}^o = k_s G_{13}^0, Q_{66}^o = G_{12}^0 \end{aligned} \quad (17)$$

where k_s is shear correction factor. The strain energy Π for a circular annular sandwich plate can be written as follows

$$\Pi = \left(U^b + U^c + U^t + V - T^b - T^c - T^t\right) \quad (18)$$

where T^b, T^c, T^t, U^b, U^c, U^t and V are kinetic and strain energies of the bottom, core and top layer in an annular sandwich plate, and external work, respectively. The kinetic energy of the sandwich plate can be expressed as follows

$$\begin{aligned} T &= \frac{1}{2}\sum_{o=t,c,b}\int_{r_i}^{r_o}\int_0^{2\pi}\int_{-h/2}^{h/2}\left(\rho^o\dot{u}^2 + \rho^o\dot{v}^2 + \rho^o\dot{w}^2\right) r dz d\theta dr \\ &= \frac{1}{2}\sum_{o=t,c,b}\int_{r_i}^{r_o}\int_0^{2\pi}\int_{-h/2}^{h/2}\left(\rho^o\left[\dot{u}_0^o + f(z)\dot{\alpha}^o\right]^2\right. \\ &\quad \left. + \rho^o\left[\dot{v}_0^o + f(z)\dot{\beta}^o\right]^2 + \rho^o\left[\dot{w}_0^o\right]^2\right) r dz d\theta dr \end{aligned} \quad (19)$$

where upper index (⊔) indicates $\partial/\partial t$. The strain energy based on MCST can be written as follows

$$\begin{aligned} U &= \frac{1}{2}\sum_{o=t,c,b}\int_{r_i}^{r_o}\int_0^{2\pi}\int_{-h/2}^{h/2}\left(\sigma_{ij}^o\varepsilon_{ij}^o + m_{ij}^o\chi_{ij}^o\right) r dz\, d\theta dr \\ &= \frac{1}{2}\sum_{o=t,c,b}\int_{r_i}^{r_o}\int_0^{2\pi}\int_{-h/2}^{h/2}\begin{pmatrix} \sigma_{rr}^o\varepsilon_{rr}^o + \sigma_{\theta\theta}^o\varepsilon_{\theta\theta}^o + 2\sigma_{r\theta}^o\varepsilon_{r\theta}^o + 2\sigma_{rz}^o\varepsilon_{rz}^o + 2\sigma_{z\theta}^o\varepsilon_{z\theta}^o \\ +m_{rr}^o\chi_{rr}^o + m_{\theta\theta}^o\chi_{\theta\theta}^o + m_{zz}^o\chi_{zz}^o + 2m_{r\theta}^o\chi_{r\theta}^o \\ +2m_{z\theta}^o\chi_{z\theta}^o + 2m_{rz}^o\chi_{rz}^o \end{pmatrix} r dz\, d\theta dr \end{aligned} \quad (20)$$

$$\begin{aligned} &m_{ij}^o = 2Gl^2\chi_{ij}^o, \quad \chi_{ij} = \frac{1}{2}\left(\vartheta_{i,j}^o + \vartheta_{j,i}^o\right), \quad \vartheta^o = \frac{1}{2}curl\left(u^o\right), \\ &\vartheta_r^o = \frac{1}{2}\left(\frac{\partial w^o}{\partial\theta} - \frac{\partial v^o}{\partial z}\right), \vartheta_\theta^o = \frac{1}{2}\left(-\frac{\partial w^o}{\partial r} + \frac{\partial u^o}{\partial z}\right), \vartheta_z^o = \frac{1}{2}\left(-\frac{\partial u^o}{\partial\theta} + \frac{\partial v^o}{\partial r}\right) \end{aligned} \quad (21)$$

where χ_{ij}^O is symmetric rotation gradient tensor of annular sandwich plate.

In this article, the value of material length scale parameter (l) is approximately assumed to be equal to 15 μm.

Substituting Eqs. (14) into Eqs. (21) yields the equations for symmetric rotation gradient tensor as follows

$$\begin{aligned} &\chi_{rr}^o = -\frac{\partial f(z)}{2\partial z}\frac{\partial\beta^0}{\partial r}, \chi_{\theta\theta}^o = 0, \chi_{zz}^o = \frac{\partial f(z)}{2\partial z}\frac{\partial\beta^o}{\partial r},. \\ &\chi_{r\theta}^o = \frac{1}{2}\left(-\frac{\partial^2 w_0^o}{2\partial r^2} + \frac{\partial f(z)}{2\partial z}\frac{\partial\alpha^o}{\partial r}\right), \\ &\chi_{\theta z}^o = \frac{\partial^2 f(z)}{4\partial z^2}\alpha^o, \chi_{rz}^o = \frac{1}{4}\left(\frac{\partial^2 v_0^o}{\partial r^2} + f(z)\frac{\partial^2\beta^o}{\partial r^2} - \frac{\partial^2 f(z)}{\partial z^2}\beta^o\right) \end{aligned} \quad (22)$$

5. Ritz method

The following equations can be considered for the displacement fields of the microcomposite sandwich plate according to Ritz solution

$$\begin{aligned} &u^o(r,\theta,z) = \bar{U}^o(R)\cos(n\theta), \alpha(r,\theta,z) = \bar{A}^o(R)\cos(n\theta), \\ &v^o(r,\theta,z) = \bar{V}^o(R)\sin(n\theta), \beta(r,\theta,z) = \bar{B}^o(R)sin(n\theta), \\ &w^o(r,\theta,z) = \bar{W}^o(R)\cos(n\theta) \end{aligned} \quad (23)$$

The amplitude of displacements can be expressed as (Zhou *et al*. 2003)

$$\bar{U}^0(R) = a_i F_1(R)F_2(R)\sum_{i=1}^{I}\cos\left[(i-1)\cos^{-1}(R)\right], \quad (24)$$

Table 1 Trial functions for different boundary conditions (Zhou *et al*. 2003)

Boundary conditions	$F_1(R)$	$F_2(R)$	$F_3(R)$	$F_4(R)$	$F_5(R)$	$F_6(R)$
Clamped	1+R	1-R	1+R	1-R	1+R	1-R
Simply supported	1	1	1+R	1-R	1+R	1-R
Free	1	1	1	1	1	1

$$\begin{aligned}
&\bar{\mathrm{A}}^0(R)=b_iF_1(R)F_2(R)\sum_{i=1}^{I}\cos\left[(i-1)\cos^{-1}(R)\right],\\
&\bar{V}^0(R)=c_iF_3(R)F_4(R)\sum_{i=1}^{I}\cos\left[(i-1)\cos^{-1}(R)\right],\\
&\bar{\mathrm{B}}^0(R)=d_iF_3(R)F_4(R)\sum_{i=1}^{I}\cos\left[(i-1)\cos^{-1}(R)\right],\\
&\bar{W}^0(R)=e_iF_5(R)F_6(R)\sum_{i=1}^{I}\cos\left[(i-1)\cos^{-1}(R)\right]
\end{aligned} \tag{24}$$

a_i, b_i, c_i, d_i, e_i are unknown Ritz coefficients and $\bar{U}^o(R)$, $\bar{A}^o(R)$, $\bar{V}^o(R)$, $\bar{\mathrm{B}}^0(R)$ and $\bar{W}^0(R)$ are the corresponding Ritz trial functions. For the axisymmetric circular annular the sandwich nanocomposite plate *n* is equal to zero. *I* is the truncation orders of the Chebyshev polynomial series. $F_i(R)$ is the function that leads to satisfying boundary conditions.

For simplicity of mathematical formulation, following dimensionless relations are considered as follows

$$R=\frac{2r}{\bar{r}}-\delta,\bar{z}=\frac{2z}{h} \tag{25}$$

where, $\bar{r}=r_o-r_i$ and $\delta=(r_o+r_i)/(r_o-r_i)$.

Trial functions for different boundary conditions are shown in Table 1. (Zhou *et al*. 2003). The abbreviations of C, S, and F denote clamped, simply supported, and free boundary conditions, respectively. Using Eqs. (21), (22) and (25), the strain energy can be written as follows

$$U=\frac{1}{2}\sum_{o=b,c,t}\int_{-1}^{1}\int_{-1}^{1}\begin{pmatrix}\left(Q_{11}^o\varepsilon_r^o+Q_{11}^o\varepsilon_\theta^o\right)\varepsilon_r^o+\left(Q_{12}^o\varepsilon_r^o+Q_{22}^o\varepsilon_\theta^o\right)\varepsilon_\theta^o+2Q_{66}^o\varepsilon_{r\theta}^o\varepsilon_{r\theta}^o+\\ 2Q_{55}^o\varepsilon_{rz}^o\varepsilon_{rz}^o+2Q_{44}^o\varepsilon_{z\theta}^o\varepsilon_{z\theta}^o+2Gl_2^2\chi_{rr}^o\chi_{rr}^o+2Gl_2^2\chi_{\theta\theta}^o\chi_{\theta\theta}^o+\\ 2Gl_2^2\chi_{zz}^o\chi_{zz}^o+4Gl_2^2\chi_{r\theta}^o\chi_{r\theta}^o+4Gl_2^2\chi_{\theta z}^o\chi_{\theta z}^o+4Gl_2^2\chi_{rz}^o\chi_{rz}^o\end{pmatrix}2\pi(R+\delta)dRd\bar{z} \tag{26}$$

Strain and symmetric rotation gradient tensor in Ritz form can be defined as follows

$$\begin{aligned}
&s_1=\bar{z},s_2=1,s_3=0\\
&\varepsilon_{rr}^o=\frac{\partial\bar{U}^o}{\partial R}+s_1\frac{\partial\bar{\mathrm{A}}^o}{\partial r},\varepsilon_{\theta\theta}^o=\frac{1}{R+\delta}\left(\bar{U}^o+s_1\bar{\mathrm{A}}^o\right),\\
&\varepsilon_{r\theta}^o=-\frac{1}{2R+2\delta}\left(\bar{V}^o+s_1\bar{\mathrm{B}}^o\right)+\frac{1}{2}\left(\frac{\partial\bar{V}^o}{\partial R}+s_1\frac{\partial\bar{\mathrm{B}}^o}{\partial r}\right)\\
&\varepsilon_{rz}^o=\frac{1}{2}\left(s_2\partial\bar{\mathrm{A}}^o+\frac{\partial\bar{W}^o}{\partial R}\right),\varepsilon_{\theta z}^o=\frac{1}{2}\left(s_2\bar{\mathrm{B}}^o\right),\\
&\chi_{rr}^o=-s_2\frac{\partial\bar{\mathrm{B}}^o}{\partial R},,\chi_{\theta\theta}^o=0,\chi_{zz}^o=s_2\frac{\partial\bar{\mathrm{B}}^o}{\partial R},\\
&\chi_{r\theta}^o=\frac{1}{2}\left(-\frac{\partial^2\bar{W}^o}{\partial R^2}+s_2\frac{\partial\bar{\mathrm{A}}^o}{\partial R}\right),\\
&\chi_{\theta z}^o=s_3\bar{\mathrm{A}}^o/4,\chi_{rz}^o=\frac{1}{4}\left(\frac{\partial^2\bar{V}^o}{\partial R^2}+s_1\frac{\partial^2\bar{\mathrm{B}}^o}{\partial R^2}+s_3\bar{\mathrm{B}}^o\right)
\end{aligned} \tag{27}$$

Also, the following relations for strain and kinetic energies can be defined as follows

$$U=\frac{1}{2}\sum_{o=b,c,t}\int_{-1}^{1}\int_{-1}^{1}\begin{pmatrix}Q_{11}^o\left[\frac{\partial\bar{U}^o}{\partial R}+s_1\frac{\partial\bar{\mathrm{A}}^o}{\partial r}\right]^2+Q_{22}^o\left[\frac{1}{R+\delta}\left(\bar{U}^o+s_1\bar{\mathrm{A}}^o\right)\right]^2+2Q_{12}^o\left[\frac{\partial\bar{U}^o}{\partial R}+s_1\frac{\partial\bar{\mathrm{A}}^o}{\partial r}\right]\left[\frac{1}{R+\delta}\left(\bar{U}^o+s_1\bar{\mathrm{A}}^o\right)\right]+\\ 2Q_{66}^o\left[-\frac{1}{2R+2\delta}\left(\bar{V}^o+s_1\bar{\mathrm{B}}^o\right)+\frac{1}{2}\left(\frac{\partial\bar{V}^o}{\partial R}+s_1\frac{\partial\bar{\mathrm{B}}^o}{\partial r}\right)\right]^2+2Q_{55}^o\left[\frac{1}{2}\left(s_2\partial\bar{\mathrm{A}}^o+\frac{\partial\bar{W}^o}{\partial R}\right)\right]^2+\\ 2Q_{44}^o\left[\frac{1}{2}\left(s_2\bar{\mathrm{B}}^o\right)\right]^2+2Gl_2^2\left[-s_2\frac{\partial\bar{\mathrm{B}}^o}{\partial R}\right]^2+2Gl_2^2\left[s_2\frac{\partial\bar{\mathrm{B}}^o}{\partial R}\right]^2+4Gl_2^2\left[\frac{1}{2}\left(-\frac{\partial^2\bar{W}^o}{\partial R^2}+s_2\frac{\partial\bar{\mathrm{A}}^o}{\partial R}\right)\right]^2+\\ 4Gl_2^2\left[s_3\bar{\mathrm{A}}^o/4\right]^2+4Gl_2^2\left[\frac{1}{4}\left(\frac{\partial^2\bar{V}^o}{\partial R^2}+s_1\frac{\partial^2\bar{\mathrm{B}}^o}{\partial R^2}+s_3\bar{\mathrm{B}}^o\right)\right]^2+\end{pmatrix}2\pi(R+\delta)dRd\bar{z} \tag{28}$$

$$\begin{aligned}T=\frac{1}{2}\sum_{o=b,c,t}\int_{-1}^{1}\int_{-1}^{1}\Bigg(\Bigg(\rho^o\left[\dot{u}_0^o+f(z)\dot{\alpha}^o\right]^2\\ +\rho^o\left[\dot{v}_0^o+f(z)\dot{\beta}^o\right]^2+\rho^o\left[\dot{w}_0^o\right]^2\Bigg)\Bigg)2\pi(R+\delta)dRd\bar{z}\end{aligned} \tag{29}$$

Substituting of Eqs. (23), (24) and (27) into Eqs. (28) and (29) yields the following equations

$$U=\sum_{o=b,c,t}\int_{-1}^{1}\int_{-1}^{1}\begin{pmatrix}Q_{11}^o\left[(a_i+s_1b_i)G_2(R)\right]^2+Q_{22}^o\left[\frac{(a_i+s_1b_i)G_1(R)}{R+\delta}\right]^2+2Q_{55}^o\left[\frac{1}{2}\left(s_2b_iG_1(R)+e_iG_8(R)\right)\right]^2+\\ 2Q_{44}^o\left[\frac{1}{2}s_2d_iG_4(R)\right]^2+2Q_{12}^o\left[(a_i+s_1b_i)G_2(R)\right]\left[\frac{(a_i+s_1b_i)G_1(R)}{R+\delta}\right]+\\ 2Q_{66}^o\left[-\frac{(c_i+s_1d_i)G_4(R)}{2R+2\delta}+\frac{1}{2}\left((c_i+s_1d_i)G_5(R)\right)\right]^2+2Gl_2^2\left[s_2d_iG_5(R)\right]^2+\\ 4Gl_2^2\left[\frac{1}{2}\left(-e_iG_9(R)+s_2b_iG_2(R)\right)\right]^2+4Gl_2^2\left[s_3b_iG_1(R)/4\right]^2+\\ 4Gl_2^2\left[\frac{1}{4}\left(c_iG_6(R)+s_1d_iG_6(R)+s_3d_iG_4(R)\right)\right]^2\end{pmatrix}2\pi(R+\delta)dRd\bar{z} \tag{30}$$

$$\begin{aligned}&T=\frac{1}{2}\sum_{o=b,c,t}\int_{-1}^{1}\int_{-1}^{1}\left(\left(\rho^o\left[\bar{U}^o+f(z)\bar{\mathrm{A}}^o\right]^2+\rho^o\left[\bar{W}^o\right]^2\right)\right)2\pi(R+\delta)dRd\bar{z}\\ &T=\frac{1}{2}\sum_{o=b,c,t}\int_{-1}^{1}\int_{-1}^{1}\begin{pmatrix}\rho^o\left[a_iF_1(R)F_2(R)G(R)+f(z)b_iF_1(R)F_2(R)G(R)\right]^2+\\ \rho^o\left[e_iF_5(R)F_6(R)G(R)\right]^2\end{pmatrix}2\pi(R+\delta)dRd\bar{z}\end{aligned} \tag{31}$$

where

$$\begin{aligned}
&G(R)=\sum_{i=1}^{I}\cos\left[(i-1)\cos^{-1}(R)\right],\\
&G_1(R)=F_1(R)F_2(R)G(R),\\
&G_2(R)=\frac{\partial}{\partial R}\left(G_1(R)\right),G_3(R)=\frac{\partial^2}{\partial R^2}\left(G_1(R)\right),\\
&G_4(R)=F_3(R)F_4(R)G(R),\\
&G_5(R)=\frac{\partial}{\partial R}\left(G_4(R)\right),G_6(R)=\frac{\partial^2}{\partial R^2}\left(G_4(R)\right),\\
&G_7(R)=F_5(R)F_6(R)G(R),\\
&G_8(R)=\frac{\partial}{\partial R}\left(G_7(R)\right),G_9(R)=\frac{\partial^2}{\partial R^2}\left(G_7(R)\right),
\end{aligned} \tag{32}$$

The following equation can be used to obtain the motion equation of the microcomposite sandwich annular plate

$$\frac{\partial\Pi}{\partial a_i}=0,\frac{\partial\Pi}{\partial b_i}=0,\ \frac{\partial\Pi}{\partial c_i}=0,\ \frac{\partial\Pi}{\partial d_i}=0,\ \frac{\partial\Pi}{\partial e_i}=0 \tag{33}$$

Using Eqs. (18) and (33) and separating variables, the motion equations can be obtained for each Ritz constant

a_i

$$\sum_{o=b,c,t}\int_{-1}^{1}\int_{-1}^{1}\left(\begin{array}{l} Q_{11}^{o}\left[G_2(R)\right]^2+Q_{22}^{o}\left[\dfrac{G_1(R)}{R+\delta}\right]^2 \\ +2Q_{12}^{o}\left[G_2(R)\right]\left[\dfrac{G_1(R)}{R+\delta}\right] \\ +2Q_{12}^{o}\left[G_2(R)\right]\left[\dfrac{G_1(R)}{R+\delta}\right] \end{array}\right)2\pi\left(a_i+s_1b_i\right)\left(R+\delta\right)dRd\overline{z} \tag{34}$$

b_i

$$\begin{aligned}&\sum_{o=b,c,t}\int_{-1}^{1}\int_{-1}^{1}\left(\begin{array}{l} Q_{11}^{o}\left(a_i+s_1b_i\right)s_1\left[G_2(R)\right]^2+ \\ Q_{22}^{o}\left(a_i+s_1b_i\right)s_1\left[\dfrac{G_1(R)}{R+\delta}\right]^2+ \\ 2Q_{12}^{o}\left(a_i+s_1b_i\right)s_1\left[G_2(R)\right]\left[\dfrac{G_1(R)}{R+\delta}\right]+ \\ \dfrac{1}{2}Q_{55}^{o}\left(s_2G_1(R)\right)\left[\left(s_2b_iG_1(R)+G_8(R)\right)\right]+ \end{array}\right)2\pi\left(R+\delta\right)dRd\overline{z} \\ &+\sum_{o=b,c,t}\int_{-1}^{1}\int_{-1}^{1}\left(\begin{array}{l} 2Gl_2^2\left[s_2G_2(R)\right]\left[\dfrac{1}{2}\left(\begin{array}{l}-\dfrac{\partial^2}{\partial R^2}\left(e_iG_7(R)\right)+ \\ s_2\dfrac{\partial}{\partial R}\left(b_iG_1(R)\right)\end{array}\right)\right]+ \\ b_iGl_2^2\left[s_3G_1(R)\right]^2 \end{array}\right)2\pi\left(R+\delta\right)dRd\overline{z}\end{aligned} \tag{35}$$

c_i

$$\begin{aligned}&\sum_{o=b,c,t}\int_{-1}^{1}\int_{-1}^{1}\left(\frac{1}{4}Gl_2^2\left[\left(\begin{array}{l}\dfrac{\partial^2}{\partial R^2}\left(c_iG_4(R)\right)+ \\ s_1\dfrac{\partial^2}{\partial R^2}\left(d_iG_4(R)\right)+s_3\left(d_iG_4(R)\right)\end{array}\right)\right]\times\left(G_6(R)\right)\right)2\pi\left(R+\delta\right)dRd\overline{z} \\ &+\sum_{o=b,c,t}\int_{-1}^{1}\int_{-1}^{1}\left(2Q_{66}^{o}\left[-\frac{G_4(R)}{2R+2\delta}+\frac{1}{2}\left(G_5(R)\right)\right]^2+\right)2\pi\left(c_i+s_1d_i\right)\left(R+\delta\right)dRd\overline{z}\end{aligned} \tag{36}$$

d_i

$$\begin{aligned}&\sum_{o=b,c,t}\int_{-1}^{1}\int_{-1}^{1}\left(\begin{array}{l} +2d_iGl_2^2\left[s_2G_5(R)\right]^2+ \\ 4Gl_2^2\left[\dfrac{1}{4}\left(\begin{array}{l}\dfrac{\partial^2}{\partial R^2}\left(c_iG_4(R)\right)+ \\ s_1\dfrac{\partial^2}{\partial R^2}\left(d_iG_4(R)\right)+s_3\left(d_iG_4(R)\right)\end{array}\right)\right]\times \\ \left[\dfrac{1}{4}\left(s_1G_6(R)+s_3G_4(R)\right)\right] \end{array}\right)2\pi\left(R+\delta\right)dRd\overline{z} \\ &+\sum_{o=b,c,t}\int_{-1}^{1}\int_{-1}^{1}\left(\begin{array}{l} 2s_1\left(c_i+s_1d_i\right)Q_{66}^{o}\left[-\dfrac{G_4(R)}{2R+2\delta}+\dfrac{1}{2}\left(G_5(R)\right)\right]^2+ \\ d_iQ_{44}^{o}\left[\left(s_2G_4(R)\right)\right]^2 \end{array}\right)2\pi\left(R+\delta\right)dRd\overline{z}\end{aligned} \tag{37}$$

e_i

$$\begin{aligned}&\frac{1}{2}\sum_{o=b,c,t}\int_{-1}^{1}\int_{-1}^{1}\left(4Gl_2^2\left[\frac{1}{2}\left(-\frac{\partial^2}{\partial R^2}\left(e_iG_7(R)\right)+s_2\frac{\partial}{\partial R}\left(b_iG_1(R)\right)\right)\right]\times\left(-\frac{1}{2}G_9(R)\right)\right)2\pi\left(R+\delta\right)dRd\overline{z} \\ &+\sum_{o=b,c,t}\int_{-1}^{1}\int_{-1}^{1}\left(2Q_{55}^{o}\left[\frac{1}{2}\left(s_2b_iG_1(R)+\frac{\partial}{\partial R}\left(e_iG_7(R)\right)\right)\right]\times\left[\frac{1}{2}\left(G_8(R)\right)\right]+\right)2\pi\left(R+\delta\right)dRd\overline{z}\end{aligned} \tag{38}$$

The matrix form of the motion equations can be expressed as follows

$$\left[K-M\omega^2\right]\left\{\begin{array}{c}a_i\\b_i\\c_i\\d_i\\e_i\end{array}\right\}=0 \tag{39}$$

The stiffness and mass coefficients can be derived as the following form

$$\begin{aligned}
K_{11}&=\sum_{o=b,c,t}\int_{-1}^{1}\int_{-1}^{1}\left(\begin{array}{l} Q_{11}^{o}\left[G_2(R)\right]^2+Q_{22}^{o}\left[\dfrac{G_1(R)}{R+\delta}\right]^2+2Q_{12}^{o}\left[G_2(R)\right]\left[\dfrac{G_1(R)}{R+\delta}\right] \\ +2Q_{12}^{o}\left[G_2(R)\right]\left[\dfrac{G_1(R)}{R+\delta}\right] \end{array}\right)2\pi\left(R+\delta\right)dRd\overline{z} \\
K_{12}&=\sum_{o=b,c,t}\int_{-1}^{1}\int_{-1}^{1}\left(\begin{array}{l} Q_{11}^{o}s_1^{o}\left[G_2(R)\right]^2+Q_{22}^{o}s_1^{o}\left[\dfrac{G_1(R)}{R+\delta}\right]^2+2Q_{12}^{o}\left[G_2(R)\right]\left[\dfrac{G_1(R)}{R+\delta}\right] \\ +2Q_{12}^{o}\left[G_2(R)\right]\left[\dfrac{G_1(R)}{R+\delta}\right] \end{array}\right)2\pi s_1^{o}\left(R+\delta\right)dRd\overline{z} \\
M_{11}&=\sum_{o=b,c,t}\int_{-1}^{1}\int_{-1}^{1}\left(\rho^{o}\left[G_1(R)\right]^2\right)2\pi\left(R+\delta\right)dRd\overline{z} \\
M_{12}&=\sum_{o=b,c,t}\int_{-1}^{1}\int_{-1}^{1}\left(\rho^{o}f(z)G_1(R)^2\right)2\pi\left(R+\delta\right)dRd\overline{z}
\end{aligned} \tag{40}$$

$$\begin{aligned}
K_{21}&=\sum_{o=b,c,t}\int_{-1}^{1}\int_{-1}^{1}\left(\begin{array}{l} Q_{11}^{o}s_1^{o}\left[G_2(R)\right]^2+Q_{22}^{o}s_1^{o}\left[\dfrac{G_1(R)}{R+\delta}\right]^2+ \\ 2Q_{12}^{o}s_1^{o}\left[G_2(R)\right]\left[\dfrac{G_1(R)}{R+\delta}\right]+ \end{array}\right)2\pi\left(R+\delta\right)dRd\overline{z} \\
K_{22}&=\sum_{o=b,c,t}\int_{-1}^{1}\int_{-1}^{1}\left(\begin{array}{l} Q_{11}^{o}s_1^{o}s_1^{o}\left[G_2(R)\right]^2+Q_{22}^{o}s_1^{o}s_1^{o}\left[\dfrac{G_1(R)}{R+\delta}\right]^2+ \\ 2Q_{12}^{o}s_1^{o}s_1^{o}\left[G_2(R)\right]\left[\dfrac{G_1(R)}{R+\delta}\right]+ \\ 2Q_{55}^{o}\left[\dfrac{1}{2}s_2^{o}G_1(R)\right]\left[\dfrac{1}{2}s_2^{o}G_1(R)\right]+ \\ 2Gl_2^2\left[\left(+s_2^{o}G_2(R)\right)\right]\left[\dfrac{1}{2}\left(s_2^{o}G_2(R)\right)\right]+Gl_2^2\left[s_3^{o}G_1(R)\right]^2 \end{array}\right)2\pi\left(R+\delta\right)dRd\overline{z} \\
K_{25}&=\sum_{o=b,c,t}\int_{-1}^{1}\int_{-1}^{1}\left(\begin{array}{l} 2Q_{55}^{o}\left[\dfrac{1}{2}\left(s_2^{o}G_7(R)\right)\right]\left[\dfrac{1}{2}\left(G_8(R)\right)\right]+ \\ 2Gl_2^2\left[\left(+s_2^{o}G_2(R)\right)\right]\left[\dfrac{1}{2}\left(-G_9(R)\right)\right]+ \end{array}\right)2\pi\left(R+\delta\right)dRd\overline{z} \\
M_{21}&=\sum_{o=b,c,t}\int_{-1}^{1}\int_{-1}^{1}\left(\rho^{o}f(z)G_1(R)^2\right)2\pi\left(R+\delta\right)dRd\overline{z} \\
M_{22}&=\sum_{o=b,c,t}\int_{-1}^{1}\int_{-1}^{1}\left(\rho^{o}\left[f(z)G_7(R)\right]^2\right)2\pi\left(R+\delta\right)dRd\overline{z}
\end{aligned} \tag{41}$$

$$\begin{aligned}
K_{33}&=\sum_{o=b,c,t}\int_{-1}^{1}\int_{-1}^{1}\left(\begin{array}{l} 2Q_{66}^{o}\left[-\dfrac{G_4(R)}{2R+2\delta}+\dfrac{1}{2}\left(G_5(R)\right)\right]^2+ \\ 4Gl_2^2\left[\dfrac{1}{4}\left(G_6(R)\right)\right]\left[\dfrac{1}{4}\left(G_6(R)\right)\right]+ \end{array}\right)2\pi\left(R+\delta\right)dRd\overline{z} \\
K_{34}&=\sum_{o=b,c,t}\int_{-1}^{1}\int_{-1}^{1}\left(\begin{array}{l} 2s_1^{0}Q_{66}^{o}\left[-\dfrac{G_4(R)}{2R+2\delta}+\dfrac{1}{2}\left(G_5(R)\right)\right]^2+ \\ 4Gl_2^2\left[\dfrac{1}{4}\left(s_1^{0}G_6(R)+s_3^{0}G_4(R)\right)\right]\left[\dfrac{1}{4}\left(G_6(R)\right)\right] \end{array}\right)2\pi\left(R+\delta\right)dRd\overline{z} \\
M_{33}&=\sum_{o=b,c,t}\int_{-1}^{1}\int_{-1}^{1}\left(\rho^{o}G_4(R)^2\right)2\pi\left(R+\delta\right)dRd\overline{z} \\
M_{34}&=\sum_{o=b,c,t}\int_{-1}^{1}\int_{-1}^{1}\left(\rho^{o}\left[f(z)G_4(R)\right]^2\right)2\pi\left(R+\delta\right)dRd\overline{z}
\end{aligned} \tag{42}$$

$$\begin{aligned}
K_{43}&=\sum_{o=b,c,t}\int_{-1}^{1}\int_{-1}^{1}\left(\begin{array}{l} 2s_1^{o}Q_{66}^{o}\left[-\dfrac{G_4(R)}{2R+2\delta}+\dfrac{1}{2}\left(G_5(R)\right)\right]^2+ \\ 4Gl_2^2\left[\dfrac{1}{4}\left(G_6(R)\right)\right]\left[\dfrac{1}{4}\left(s_1^{o}G_6(R)+s_3^{o}G_4(R)\right)\right] \end{array}\right)2\pi\left(R+\delta\right)dRd\overline{z} \\
K_{44}&=\sum_{o=b,c,t}\int_{-1}^{1}\int_{-1}^{1}\left(\begin{array}{l} 2s_1^{o}s_1^{o}Q_{66}^{o}\left[-\dfrac{G_4(R)}{2R+2\delta}+\dfrac{1}{2}\left(G_5(R)\right)\right]^2+ \\ 2s_2^{o}Q_{44}^{o}\left[G_5(R)\right]^2+2s_2^{o}Gl_2^2\left[G_5(R)\right]^2+ \\ 4Gl_2^2\left[\dfrac{1}{4}\left(s_1^{o}G_6(R)+s_3^{o}G_4(R)\right)\right]\left[\dfrac{1}{4}\left(s_1^{o}G_6(R)+s_3^{o}G_4(R)\right)\right] \end{array}\right)2\pi\left(R+\delta\right)dRd\overline{z} \\
M_{43}&=\sum_{o=b,c,t}\int_{-1}^{1}\int_{-1}^{1}\left(\rho^{o}f(z)G_4(R)\right)2\pi\left(R+\delta\right)dRd\overline{z} \\
M_{44}&=\sum_{o=b,c,t}\int_{-1}^{1}\int_{-1}^{1}\left(\rho^{o}\left[f(z)G_4(R)\right]^2\right)2\pi\left(R+\delta\right)dRd\overline{z}
\end{aligned} \tag{43}$$

$$\begin{aligned}
K_{52}&=\sum_{o=b,c,t}\int_{-1}^{1}\int_{-1}^{1}\left(\begin{array}{l} 2Q_{55}^{o}\left[\dfrac{1}{2}s_2^{o}G_1(R)\right]\times\left[\dfrac{1}{2}G_8(R)\right]+ \\ 4Gl_2^2\left[\dfrac{1}{2}s_2^{o}G_2(R)\right]\left[-\dfrac{1}{2}G_9(R)\right] \end{array}\right)2\pi\left(R+\delta\right)dRd\overline{z} \\
K_{55}&=\sum_{o=b,c,t}\int_{-1}^{1}\int_{-1}^{1}\left(2Q_{55}^{o}\left[\frac{1}{2}G_8(R)\right]^2+4Gl_2^2\left[\frac{1}{2}G_9(R)\right]^2\right)2\pi\left(R+\delta\right)dRd\overline{z} \\
M_{55}&=\sum_{o=b,c,t}\int_{-1}^{1}\int_{-1}^{1}\left(\rho^{o}G_7(R)^2\right)2\pi\left(R+\delta\right)dRd\overline{z}
\end{aligned} \tag{44}$$

6. Results and discussions

Free vibration analysis of the microcomposite annular sandwich plate with carbon nanotube reinforced composite (CNTRC) facesheets and FG porous core is presented. Firstly, the used materials properties in this article are defined for three layers of the sandwich plate. Then, using the present method, the accuracy and efficiency of the approach is studied by several examples. Lastly, the effects of porosity distribution, geometrical parameters, various boundary conditions and volume fraction of carbon nanotubes on the first mode shape of free vibration characteristics of the microcomposite annular sandwich plate are also reported.

Polymethyl methacrylate (PMMA) is assumed as the matrix of facesheets that the material properties are set as follows

$$\rho = 1150(\mathrm{Kg/m^3}), \quad \upsilon = 0.34, \quad E = 2.1(\mathrm{Gpa}), \quad k_s = 1.$$

In addition, the SWCNTs are used as reinforcement of facesheets that the materials properties are set as follows

$$E_{11}^{CNT} = 5.6466\ (TPa), \quad E_{22}^{CNT} = 7.08\ (TPa)$$
$$G_{12}^{CNT} = 1.9445\ (TPa), \quad \rho = 1400\ Kg/m^3$$
$$\text{and} \quad v_{12} = 0.175.$$

Efficiency parameters for various volume fractions in mixture rule approach are tabulated in Table 2 that is used for validation and some reports (Mohammadimehr *et al*. 2018b, Shi *et al*. 2004) For other cases E-M-T approached is selected with following efficiency k_r = 30e9, l_r = 10e9, m_r = le9, n_r = 450e9, p_r = le9 (Shi *et al*. 2004).

6.1 Formulation validation

As no published results for the microcomposite annular sandwich plate with carbon naotube reinforced composite facesheets and functionally graded (FG) porous core in the open literature. In Table 3, the present results are compared with the obtained results by (Zhong *et al*. 2018) for vibration analysis ($(\Omega = (r_b^2\omega/h)\sqrt{\rho_m/E_m})$) of CNTs reinforced composite annular plate. In terms of geometrical parameters, CNTs reinforced composite annular plate with two CC and SS boundary conditions have been compared in classical theory. Moreover, natural frequency for CNTs reinforced composite annular plates with (R_b/R_a = 2, h/R_b = 0.1) are obtained by using an approach of mixtures rule.

Another comparison results of dimensionless natural frequency (Ω) with CS boundary conditions are tabulated in Table 4 that the material properties on the bottom and top facesheets are assumed as ceramic and metal, respectively. The material constants are: ρ_m = 2707 kg/m^3, E_m = 70 Gpam v_m = 0.3 and ρ_c = 700 kg/m^3, E_c = 168 Gpa, v_c = 0.3. The results show the third mode sequence number of the annular plate and some value of aspect ratios and inner-to-outer radius ratio.

Table 2 The CNTs efficiency parameters for various volume fractions in the mixture rule approach (Mohammadimehr *et al*. 2018b, Shi *et al*. 2004)

V_{CNT}^*	η_1	η_2	η_3
0.11	0.149	0.934	0.934
0.12	0.137	1.022	0.715
0.14	0.150	0.941	0.941
0.17	0.149	1.381	1.381
0.28	0.141	1.585	1.109

Table 3 Comparison of natural frequency parameters (Ω) for CNTs reinforced composite annular plates with two types of boundary conditions (R_a/R_b = 2, h/R_b = 0.1)

V_{cnt}	CC		SS	
	Present work	Zhong *et al.* 2018	Present	Zhong *et al.* 2018
0.11	34.5374	34.5169	13.608	13.7706
0.14	35.491	35.2669	13.983	14.0151
0.17	42.9253	43.1567	16.912	17.2297

Table 4 Comparison of the frequency parameters (Ω) for CNTs reinforced composite annular plates with CS boundary conditions (R_a/R_b = 2, h/R_b = 0.1)

h/R_b	R_a/R_b	Present	Wang *et al.* 2016	Guo *et al.* 2018	Zhong *et al.* 2018
0.1	0.5	195.056	194.990	194.990	194.981
	0.7	477.039	476.676	476.681	476.667
0.2	0.5	163.855	163.592	163.620	163.594
	0.7	402.652	402.009	402.073	402.011

6.2 Discussion and results

Fig. 2 depicts the dimensionless free vibration of microcomposite annular sandwich plate versus aspect ratios of R_a/R_b. Various distributions of CNT for facesheets and the uniform porous core of the sandwich plate are assumed. The obtained result shows that E-M-T and EMR with (V_{CNT} = 0.17, η_1 = 0.142, η_2 = 1.138, η_3 = 1.138) approached are quite close together instead of the H-T approach. H-T approach is quite useful in determining the properties of composites that contain discontinuous fibers oriented in the loading direction (Abdel Ghafaar 2006). Hence, E-M-T and EMR approached are chosen for the present investigation.

Fig. 3 demonstrates the effects of thickness-to-outer radius ratio changes on the dimensionless free vibration of the microcomposite annular sandwich plate for five types of boundary conditions. Uniform porous core with e_0 = 0.5 and E-M-T approached as a reinforcement of facesheets is considered. Dimensionless natural frequency parameter $\Omega = r_b\omega\sqrt{\rho h/D}$ (where D is the flexural stiffness) is used

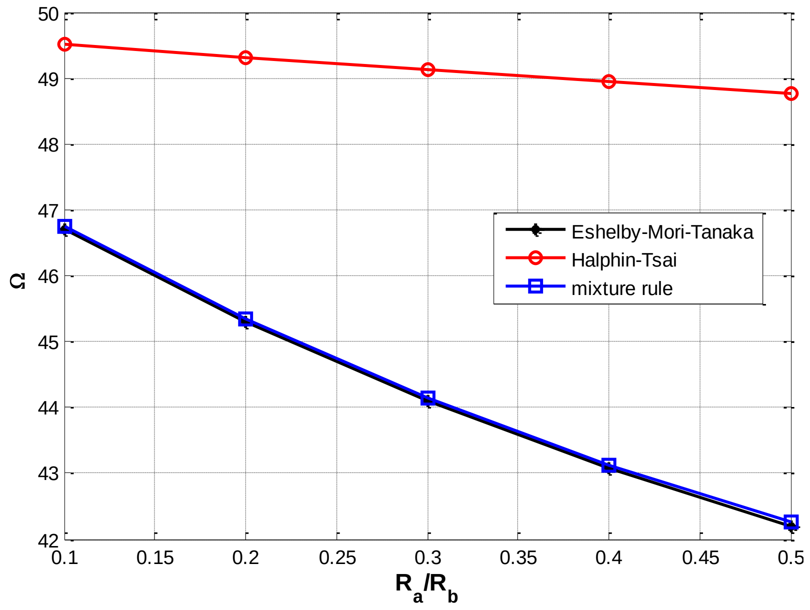

Fig. 2 Dimensionless free vibration of microcomposite annular sandwich plate versus aspect ratios of R_a/R_b for three types of CNT reinforced approached of facesheets and uniform porous core (e_0 = 0.5, h_c = 0.8h, h = 0.2R_b)

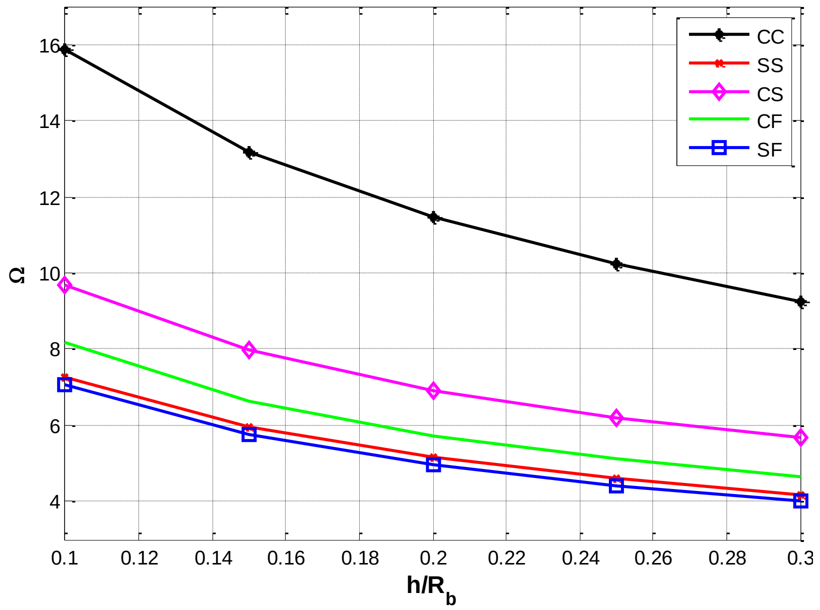

Fig. 3 The effects of boundary conditions on the dimensionless free vibration of the microcomposite annular sandwich plate vs. thickness to outer radius ratios (e_0 = 0.5, h_c = 0.8h, R_a = 0.5R_b)

for all the following results. Dimensionless natural frequencies lead to a smaller value by rising of thickness to outer radius ratios.

The effects of various porosity distributions such as (a) uniform porosity distribution; (b) non-uniform asymmetrical porosity distribution (FG-A); (c) non-uniform symmetrical porosity distribution (FG-B) on the natural frequency of the microcomposite sandwich plate with different porosity distributions in the porous core is illustrated in Figs. 4(a), (b) and (c), respectively. The result for these figures based on MCST and E-M-T approached in facesheet are obtained with assuming of C-C boundary conditions. It is found that increasing value of aspect ratios (l/h) (the ratio of material length scale parameter to thickness) enhances the natural frequency and for higher l/h, the variation rate of natural frequency leads to approximately constant which is a typical hardening behavior due to increasing of size dependent effect. Also, by increasing porosity coefficient or increasing size of the internal pores, a dimensionless free vibration decreases and the plate stiffness will be reduced. Annular sandwich plates with non-uniform porosity distribution including symmetric and asymmetric and uniform porosity distribution have the same behavior but in different ranges.

The effects of pore compressibility with uniform and non-uniform symmetric distribution on dimensionless

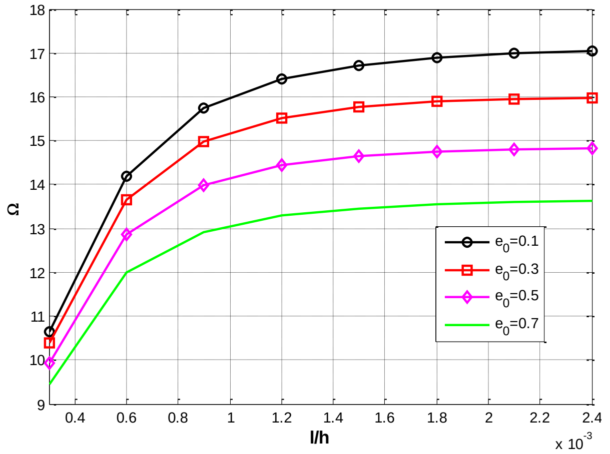

(a) Uniform porosity distribution

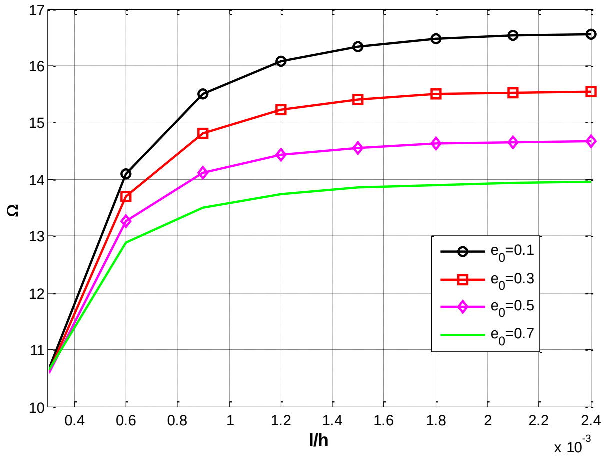

(b) Non-uniform asymmetrical porosity distribution (FG-A)

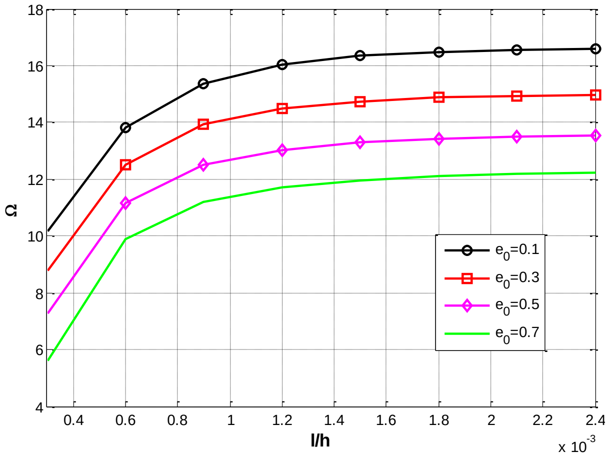

(c) Non-uniform symmetrical porosity distribution (FG-B)

Fig. 4 The effects of various porosity distributions on dimensionless natural frequency versus aspect ratios of for C-C microcomposite annular sandwich plate (h = 0.1R_b, h_c = 0.8h, R_a = 0.5R_b)

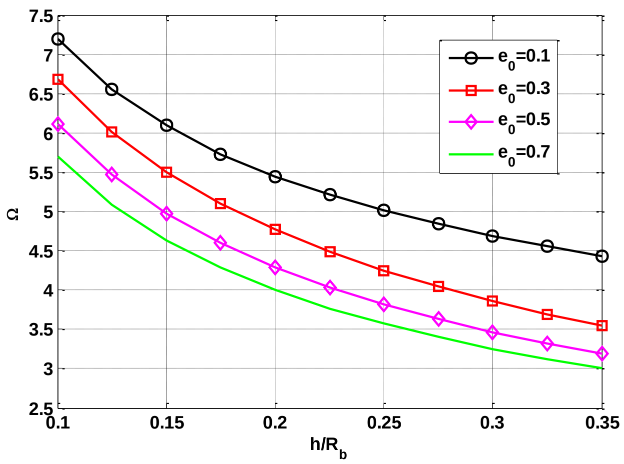

(a) Uniform porosity distribution

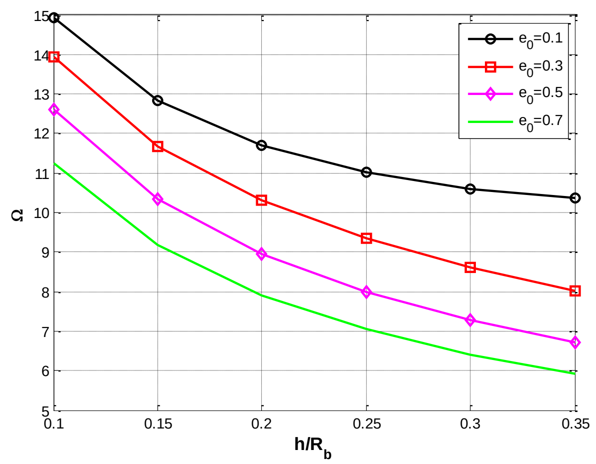

(b) Non-uniform asymmetrical porosity distribution (FG-B)

Fig. 5 Effect of various porosity distributions on the dimensionless natural frequency of the microcomposite annular sandwich plate vs. thickness to outer radius ratios predicted by MCST (l = 15 μm, h_c = 0.8h, R_a = 0.5R_b)

natural frequencies are shown in Figs. 5(a) and (b). This graph is predicted by C-C boundary conditions, E-M-T approached and MCST. These figures show that by increasing the pore compressibility and thickness to outer radius ratios, the frequency of the sandwich plate decreases.

Fig. 6 presents the dimensionless natural frequency of microcomposite annular sandwich plate for a variation range of facesheet-total thickness ratios and different pore

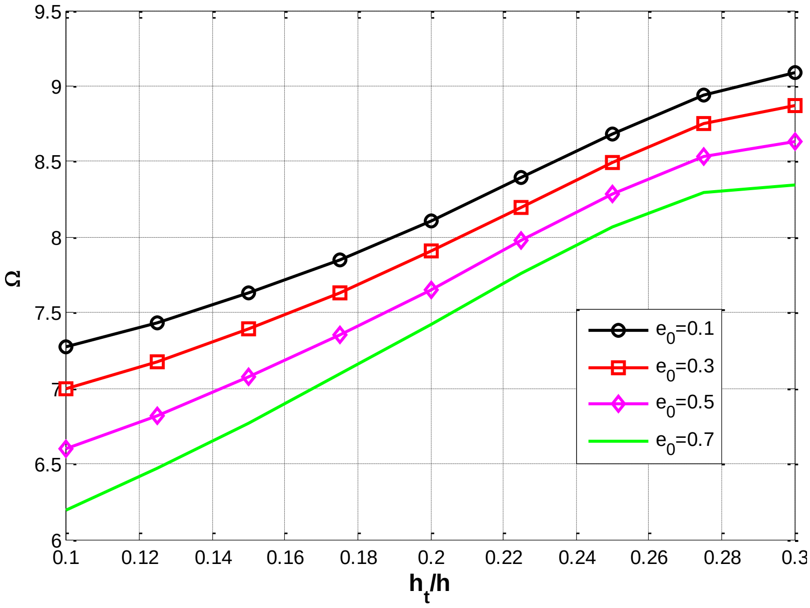

Fig. 6 The effects of boundary conditions on the dimensionless free vibration of the microcomposite annular sandwich plate vs. thickness to outer radius ratios ($h = 0.1R_b$, $l = 15\ \mu$m, $R_a = 0.5R_b$)

Table 5 The dimensionless natural frequency of annular sandwich plates for different boundary conditions and various radius ratios ($h_c/h = 0.8$)

BC	e_0	h/R_b					
		$R_a/R_b = 0.3$			$R_a/R_b = 0.5$		
		0.1	0.2	0.3	0.1	0.2	0.3
S-S	0.4	7.2009	5.2770	4.4087	7.8125	5.7232	4.7798
	0.6	6.4265	4.5978	3.7559	6.9485	4.9699	4.0587
	0.8	5.4779	3.8640	3.1288	5.9005	4.1613	3.3689
C-S	0.4	9.8084	6.9316	5.8573	9.9329	7.1956	6.0286
	0.6	9.5513	6.8408	5.6289	9.8985	7.1430	5.8633
	0.8	9.3751	6.6289	5.4041	9.5617	6.7537	5.5002
C-F	0.4	8.1955	5.8405	4.7823	8.7054	6.2028	5.0780
	0.6	7.3206	5.1553	4.1837	7.7637	5.4667	4.4358
	0.8	6.2754	4.4046	3.5688	6.6436	4.6626	3.7775
S-F	0.4	6.8977	4.8896	3.9901	7.4835	5.3029	4.3258
	0.6	6.2224	4.3754	3.5479	6.7278	4.7294	3.8385
	0.8	5.3830	3.7785	3.0627	5.7983	4.0692	3.2977

compressibility of the uniform porous core of the sandwich plate. This figure is also predicted by the C-C boundary condition and E-M-T approached based on MCST. The thickness ranges of sandwich structures facesheets are limited as $0.1 \le h_t/h \le 0.3$. Moreover, by increasing the facesheet-to-total thickness ratios, the strength of the structures leads to higher values.

Since all the graphs are drawn to C-C boundary conditions, Table 5 shows the dimensionless natural frequencies for various different boundary conditions such as (S-F, C-F, S-S, C-S), these results are demonstrated for uniform porosity distribution ($e_0 = 0.5$) and EMT approach based on MCST. The shear correction factor is defined as: $k_s = \pi^2/12$. It is shown that, dimensionless natural frequency increases with an increase of radius ratio and decreases with increasing of porosity constant and thickness to outer radius ratios.

Fig. 7 depicts the effect of h/R_b on dimensionless natural frequency of the microcomposite annular sandwich plate predicted by MCST. Carbon nanotubes reinforced composite facesheets with EMR approached ($V_{CNT} = 0.17$) and uniform porous core ($e_0 = 0.5$) are selected. Variation range of free vibration for lower ratios of h/R_b are much more than larger ratios and when these changes lead to higher values, even by changing of R_a/R_b ratios, these variations are almost constant.

The dimensionless natural frequency Ω of micro-composite annular sandwich plate with uniform porous core based on MCST and various volume fractions of CNTs with EMR approached by the material parameters that are listed in Table 2 is illustrated in Fig. 8. According to C-C boundary conditions and based on MCST, by increasing of inner to outer radius ratios and decreasing of volume fraction percentage, the dimensionless natural frequency leads to lower values.

7. Conclusions

In this research, a dimensionless natural frequency of microcomposite annular sandwich plate was developed using modified couple stress (MCST) and first order shear deformation theories (FSDT). Various porosity distributions such as (A) asymmetric, (B) symmetric, and (C) uniform are considered as the core of sandwich structures. The mechanical properties of carbon nanotubes reinforced composite facesheets are predicted by different approaches such as extended mixture rule (EMR), Eshelby-Mori-Tanaka (E-M-T), and Halpin-Tsai (H-T) and governing equations were derived by using Hamilton's principle. To

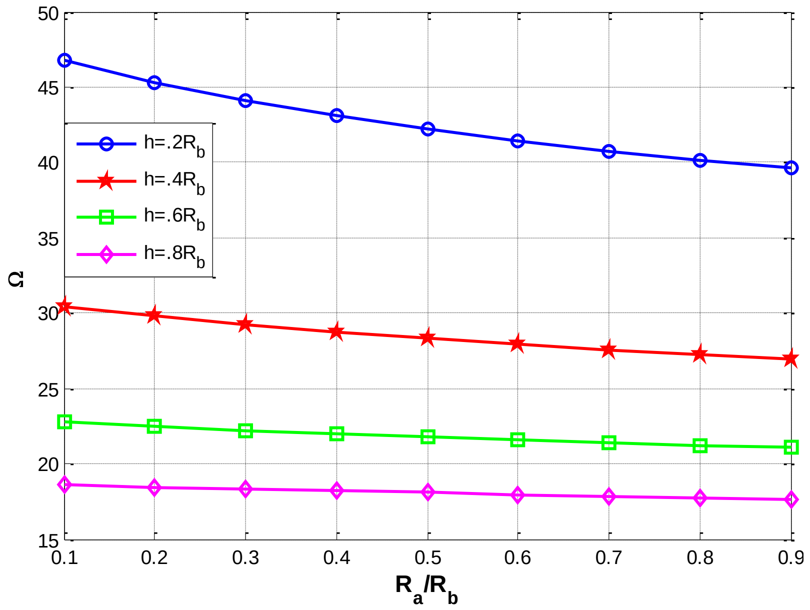

Fig. 7 Effect of on dimensionless natural frequency of microcomposite annular sandwich plate with CNTs reinforced facesheets (EMR approached) and uniform porous core predicted by MCST (e_0 = 0.5, h_c = 0.8h, V_{CNT} = 0.17)

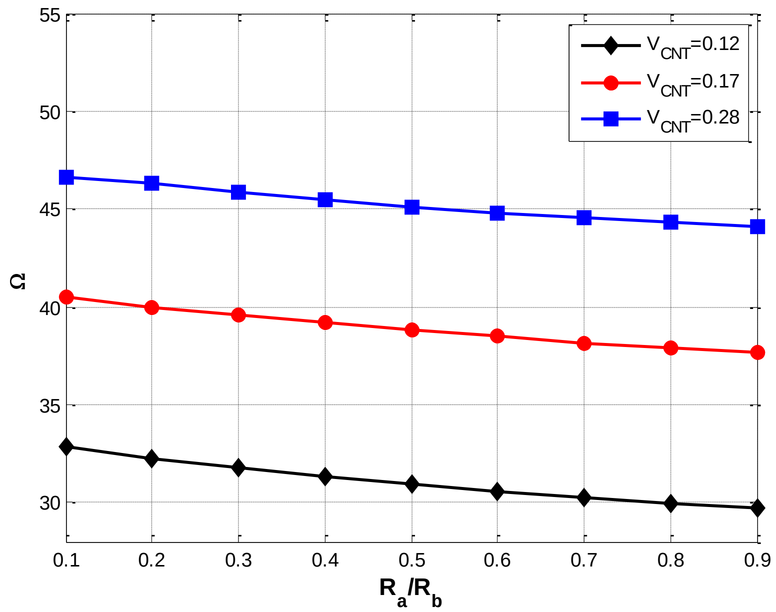

Fig. 8 Dimensionless natural frequency (Ω) of microcomposite annular sandwich plate versus inner to outer radius ratios based on MCST for various Volume Fraction of CNTs with EMR approached (e_0 = 0.5, h_c = 0.8h, h = 0.2R_b)

obtain the natural frequencies of the microcomposite annular sandwich plate, the governing equations along with different boundary conditions are solved by the Ritz method and predicted results are validated by comparing studies for CNTs reinforced annular plates with clamped and simply supported boundary conditions. Hence, the effects of material length scale parameters, various boundary conditions, aspect and inner-outer radius ratios, FG porous distributions, pore compressibility, and volume fraction of CNTs in the EMR approached on the dimensionless natural frequencies are considered.

It is observed that the effect of the pore compressibility in all kind of FG porous distributions in the core of sandwich structures leads to lower natural frequencies values but the behavior of them are not the same exactly and Ω has different range values vibration. Also increasing the value of inner-to-outer radius ratios and thickness to radius ratios leads to the lower value of dimensionless free frequencies. Furthermore, dimensionless free frequency increases by increasing of facesheet-to-total thickness ratios of the sandwich plate by considering of constant value for total thickness. Moreover, dimensionless free frequency increases by the increase of l/h ratio lead to constant free frequency values.

Acknowledgments

The authors would like to thank the referees for their valuable comments. Also, they are thankful to the Iranian Nanotechnology Development Committee for their financial support and the University of Kashan for supporting this work by Grant No. 682561/12.

References

Abdel Ghafaar, M., Mazen, A.A. and El-Mahallawy, N.A. (2006), "Application of the rule of mixtures and halpin-tsai equations to woven fabric reinforced epoxy composites", *J. Eng. Sci. Assiut Univ.*, **34**(1), 227-236.

Ahouel, M., Sid Ahmed, H.M., Bedia, E.A.A. and Tounsi, A. (2016), "Size-dependent mechanical behavior of functionally graded trigonometric shear deformable nanobeams including neutral surface position concept", *Steel Compos. Struct., Int. J.*, **20**(5), 963-981.

Al-Basyouni, K.S., Tounsi, A. and Mahmoud, S.R. (2015), "Size dependent bending and vibration analysis of functionally graded micro beams based on modified couple stress theory and neutral surface position", *Compos. Struct.*, **125**, 621-630.

Arani, A.G., Mohammadimehr, M., Saidi, A.R., Shogaei, S. and Arefmanesh, A. (2011a), "Thermal buckling analysis of double-walled carbon nanotubes considering the small-scale length effect", *Proc. IMechE, Part C, J. Mech. Eng. Sci.*, **225**(1), 248-256.

Arani, A.G., Hashemian, M., Loghman, A. and Mohammadimehr, M. (2011b), "Study of dynamic stability of the double-walled carbon nanotubes under axial loading embedded in an elastic medium by the energy method", *J. Appl. Mech. Tech. Phys.*, **52**(5), 815-824.

Arani, A.G., Mobarakeh, M.R., Shams, S. and Mohammadimehr, M. (2012), "The effect of CNT volume fraction on the magneto-thermo-electro-mechanical behavior of smart nanocomposite cylinder", *J. Mech. Sci. Technol.*, **26**(8), 2565-2572.

Ashby, M.F., Evans, T., Fleck, N.A., Hutchinson, J., Wadley, H. and Gibson L. (2000), *Metal Foams: A Design Guide*, Butterworth-Heinemann, Boston, MA, USA.

Belkorissat, I., Sid Ahmed, H.M., Bedia, E.A.A., Tounsi, A. and Hassan, S. (2015), "On vibration properties of functionally graded nano-plate using a new nonlocal refined four variable model", *Steel Compos. Struct., Int. J.*, **18**(4), 1063-1081.

Bellifa, H., Benrahou, K.H., Bousahla, A.A., Tounsi, A. and Hassan, S. (2017), "A nonlocal zeroth-order shear deformation theory for nonlinear postbuckling of nanobeams", *Struct. Eng. Mech., Int. J.*, **62**(6), 695-702.

Bellifa, H., Benrahou, K.H., Hadji, L., Houari, M.S.A. and Tounsi, A. (2018), "Bending and free vibration analysis of functionally graded plates using a simple shear deformation theory and the concept the neutral surface position", *J. Braz. Soc. Mech. Sci. Eng.*, **38**, 265-275.

Betts, C. (2012), "Benefits of metal foams and developments in modeling techniques to assess their materials behavior: a review", *Mater. Sci. Technol.*, **28**, 129-143.

Bounouara, F., Benrahou, K.H., Belkorissat, I. and Tounsi, A. (2016), "A nonlocal zeroth-order shear deformation theory for free vibration of functionally graded nanoscale plates resting on elastic foundation", *Steel Compos. Struct., Int. J.*, **20**(2), 227-249.

Bourada, M., Kaci, A., Houari, M.S.A. and Tounsi, A. (2015), "A new simple shear and normal deformations theory for functionally graded beams", *Steel Compos. Struct., Int. J.*, **18**(2), 409-423.

Chen, D., Yang, J. and Kitipornchai, S. (2015), "Elastic buckling and static bending of shear deformable functionally graded porous beam", *Compos. Struct.*, **133**, 54-61.

Chen, D., Kitipornchai, S. and Yang, J. (2016), "Nonlinear free vibration of shear deformable sandwich beam with a functionally graded porous core", *Thin-Wall. Struct.*, **107**, 39-48.

Dukhan, N. (2013), *Metal Foams: Fundamentals and Applications*, DEStech Publications, Inc Lancaster USA.

Ghorbanpour Arani, A., Rousta Navi, B. and Mohammadimehr, M. (2016), "Surface stress and agglomeration effects on nonlocal biaxial buckling polymeric nanocomposite plate reinforced by CNT using various approaches", *Adv. Compos. Mater.*, **25**(5), 423-441.

Guo, J., Shi, D., Wang, Q., Pang, F. and Liang, Q. (2018), "A domain decomposition approach for static and dynamic analysis of composite laminated curved beam with general elastic restrains", *Mech. Adv. Mater. Struct.*, 1-13.
DOI: 10.1080/15376494.2018.1432810

Halpin, J.C. and Kardos, J.L. (1976), "The Halpin –Tsaiequation: a review", *Polym. Eng. Sci.*, **16**, 344-352.

Jalaei, M.H., Ghorbanpour, Arani, A. and Tourang, H. (2018), "On the dynamic stability of viscoelastic graphene sheets", *Int. J.of En. Sci.*, **132**, 16-29.

Jasion, P. and Magnucki, K. (2013), "Global buckling of a sandwich column with metal foam core", *J. Sandw. Struct. Mater.*, 1099636213499339.

Jia, J., Zhao, J., Xu, G., Di, J., Yong, Z., Tao, Y., Fang, C., Zhang, Z., Zhang, X., Zheng, L. and Li, Q. (2011), "A comparison of the mechanical properties of fibers spun from different carbon nanotubes", *Carbon*, **49**, 1333-1339.

Karami, B., Janghorban, M. and Tounsi, A. (2018), "Variational approach for wave dispersion in anisotropic doubly-curved nanoshells based on a new nonlocal strain gradient higher order shell theory", *Thin-Wall. Struct.*, **129**, 251-264.

Ke, L.L. and Wang, Y.S. (2013), "Bending and vibration of functionally graded microbeams using a new higher order beam theory and the modified couple stress theory", *Int. J. Eng. Sci.*, **64**, 37-53.

Kong, S., Zhou, S., Nie, Z. and Wang, K. (2009), "Static and dynamic analysis of micro beams based on strain gradient elasticity theory", *Int. J. Eng. Sci.*, **47**(4), 487-498.

Lam, D.C.C., Yang, F. and Chong, A.C.M. (2003), "Experiments and theory in strain gradient elasticity", *J. Mech. Phys. Solids*, **51**, 1477-1508.

Lei, Z.X., Zhang, L.W., Liew, K.M. and Yu, J.L. (2014), "Dynamic stability analysis of carbon nanotube-reinforced functionally graded cylindrical panels using the element-free kp-Ritz method", *Compos. Struct.*, **113**, 328-338.

Lei, Z.X., Zhang, L.W. and Liew, K.M. (2015), "Free vibration analysis of laminated FG-CNT reinforced composite rectangular plates using the kp-Ritz method", *Compos. Struct.*, **127**, 245-259.

Lei, Z.X., Zhang, L.W. and Liew, K.M. (2016a), "Analysis of laminated CNT reinforced functionally graded plates using the element-free kp-Ritz method", *Compos. part B*, **84**, 211-221.

Lei, Z.X., Zhang, L.W. and Liew, K.M. (2016b), "Analysis of laminated CNT reinforced functionally graded plates using the element-free kp-Ritz method", *Compos. part B*, **85**, 140-149.

Magnucka-Blandzi, E. (2009), "Dynamic stability of a metal foam circular plate", *J. Theor. Appl. Mech.*, **47**(2), 421-433.

Magnucka-Blandzi, E. (2011), "Mathematical modeling of a rectangular sandwich plate with metal foam core", *J. Theor. Appl. Mech.*, **49**(2), 439-455.

Magnucki, K. and Stasiewicz, P. (2004), "Elastic buckling of a porous beam", *J. Theor. Appl. Mech.*, **42**(4), 859-868.

Mahi, A., Bedia, E.A. and Tounsi, A. (2015), "A new hyperbolic shear deformation theory for bending and free vibration analysis of isotropic, functionally graded sandwich and laminated composite plates", *Appl. Math. Model.*, **39**, 2489-2508.

Menasria, A., Bouhadra, A., Tounsi, A., Bousahla, A.A. and Mahmoud, S.R. (2017), "A new and simple HSDT for thermal stability analysis of FG sandwich plates", *Steel Compos. Struct., Int. J.*, **25**(2), 157-175.

Meziane, A.A., Abdelaziz, H.H. and Tounsi, A. (2014), "An efficient and simple refined theory for buckling and free vibration of exponentially graded sandwich plates under various boundary conditions", *J. Sandw. Struct. Mater.*, **16**(3), 293-318.

Mohammadimehr, M. and Alimirzaei, S. (2016), "Nonlinear static and vibration analysis of Euler-Bernoulli composite beam model reinforced by FG-SWCNT with initial geometrical imperfection using FEM", *Struct. Eng. Mech., Int. J.*, **59**(3), 431-454.

Mohammadimehr, M. and Alimirzaei, S. (2017), "Buckling and free vibration analysis of tapered FG- CNTRC micro Reddy beam under longitudinal magnetic field using FEM", *Smart Struct. Syst., Int. J.*, **19**(3), 309-322.

Mohammadimehr, M. and Mehrabi, M. (2017), "Stability and free vibration analyses of double-bonded micro composite sandwich cylindrical shells conveying fluid flow", *Appl. Math. Model.*, **47**, 685-709.

Mohammadimehr, M. and Mehrabi, M. (2018), "Electro-thermo-mechanical vibration and stability analyses of double-bonded micro composite sandwich piezoelectric tubes conveying fluid flow", *Appl. Math. Model.*, **60**, 255-272.

Mohammadimehr, M. and Rahmati, A.H. (2013), "Small scale effect on electro-thermo-mechanical vibration analysis of single-walled boron nitride nanorods under electric excitation", *Turkish J. Eng. Environ. Sci.*, **37**(1), 1-15.

Mohammadimehr, M. and Salemi, M. (2014), "Bending and buckling analysis of functionally graded Mindlin nano-plate model based on strain gradient elasticity theory", *Indian J. Sci. Res.*, **2**(2), 587-598.

Mohammadimehr, M. and Shahedi, S. (2017) "High-order buckling and free vibration analysis of two types sandwich beam including AL or PVC-foam flexible core and CNTs reinforced nanocomposite face sheets using GDQM", *Compos. Part B: Eng.*, **108**, 91-107.

Mohammadimehr, M., Saidi, A.R., Arani, A.G., Arefmanesh, A. and Han, Q. (2010), "Torsional Buckling of a DWCNT Embedded on Winkler and Pasternak Foundations Using Nonlocal Theory", *J. Mech. Sci. Tech.*, **24**(6), 1289-1299.

Mohammadimehr, M., Rousta-Navi, B. and Ghorbanpour-Arani, A. (2014), "Biaxial buckling and bending of smart nanocomposite plate reinforced by CNTs using extended mixture rule approach", *Mech. Adv. Compos. Struct.*, **1**, 17-26.

Mohammadimehr, M., Shahedi, S. and Rousta Navi, B. (2016a), "Nonlinear vibration analysis of FG-CNTRC sandwich Timoshenko beam based on modified couple stress theory subjected to longitudinal magnetic field using generalized differential quadrature method", *Proceedings of the Institution of Mechanical Engineers, Part C: Journal of Mechanical Engineering Science*, **231**(20), 3866-3885.

Mohammadimehr, M., Navi, B.R. and Arani, A.G. (2016b), "Modified strain gradient Reddy rectangular plate model for biaxial buckling and bending analysis of double-coupled piezoelectric polymeric nanocomposite reinforced by FG-SWNT", *Compos. Part B*, **87**, 132-148.

Mohammadimehr, M., Rostami, R. and Arefi, M. (2016c), "Electro-elastic analysis of a sandwich thick plate considering FG core and composite piezoelectric layers on Pasternak foundation using TSDT", *Steel Compos. Struct., Int. J.*, **20**(3), 513-544.

Mohammadimehr, M., Mohammadimehr, M.A. and Dashti, P. (2016d), "Size-dependent effect on biaxial and shear nonlinear buckling analysis of nonlocal isotropic and orthotropic micro-plate based on surface stress and modified couple stress theories using differential quadrature method (DQM)", *Appl. Math. Mech.* (English Edition), **37**(4), 529-554.

Mohammadimehr, M., Zarei, H.B., Parakandeh, A. and Arani, A.G. (2017), "Vibration analysis of double-bonded sandwich microplates with nanocomposite facesheets reinforced by symmetric and un-symmetric distributions of nanotubes under multi physical fields", *Struct. Eng. Mech., Int. J.*, **64**(3), 361-379.

Mohammadimehr, M., Emdadi, M., Afshari, H. and Rousta Navi, B. (2018a), "Bending, buckling and vibration analyses of MSGT microcomposite circular-annular sandwich plate under hydro-thermo-magneto-mechanical loadings using DQM", *Int. J. Smart Nano Mater.*, **9**(4), 223-260.

Mohammadimehr, M., Emdadi, M. and Rousta Navi, B. (2018b), "Dynamic stability analysis of microcomposite annular sandwich plate with CNT reinforced composite facesheets based on MSGT", *J. Sandw. Struct. Mater.*, DOI: org/10.1177/1099636218782770

Mojahedin, A., Jabbari, M., Khorshidvand, A.R. and Eslami, M.R. (2016), "Buckling analysis of functionally graded circular plates made of saturated porous materials based on higher order shear deformation theory", *Thin-Wall. Struct.*, **99**, 83-90.

Nguyen, H.X., Nguyen, T.N., Abdel-Wahab, M., Bordas, S.P.A., Nguyen-Xuan, H. and Vo, T.P. (2017), "A refined quasi-3D isogeometric analysis for functionally graded microplates based on the modified couple stress theory", *Comput. Methods Appl. Mech. Eng.*, **313**, 904-940.

Shi, D., Feng, X.Q. and Huang, Y.Y. (2004), "The effect of nanotube waviness and agglomeration on the elastic property of carbon nanotube-reinforced composite", *J. Eng. Mater. Technol.*, **126**, 250-257.

Şimşeka, M. and Reddy, J.N. (2014), "Bending and free vibration of functionally graded piezoelectric beam based on modified strain gradient theory", *Compos. Struct.*, **115**, 41-50.

Smith, B.H., Szyniszewski, S., Hajjar, J.F., Schafer, B.W. and Arwade, S.R. (2012), "Steel foam for structures: a review of applications, manufacturing and material properties", *J. Constr. Steel Res.*, **117**, 1-10.

Sun, C.H., Li, F., Cheng, H.M. and Lu, G.Q. (2005), "Axial Young's modulus prediction of single walled carbon nanotube arrays with diameters from nanometer to meter scales", *Appl. Phys. Lett.*, **87**, 193-201.

Ugale, V., Singh, K. and Mishra, N. (2015), "Comparative study of carbon fabric reinforced and glass fabric reinforced thin sandwich panels under impact and static loading", *J. Compos. Mater.*, **49**, 99-112.

Wang, Z.X. and Shen, H.S. (2012), "Nonlinear vibration and bending of sandwich plates with nanotube reinforced composite", *Compos. Part B*, **43**, 411-421.

Wang, B., Zhou, S., Zhao, J. and Chen, X. (2011), "A size-dependent Kirchhoff micro-plate model based on strain gradient elasticity theory", *Eur. J. Mech. A-Solid*, **30**, 517-524.

Wang, Q., Shi, D., Liang, Q. and Shi, X. (2016), "A unified solution for vibration analysis of functionally graded circular, annular and sector plates with general boundary conditions", *Compos. Part B-Eng.*, **88**, 264-294.

Wen, P.H. (2012), "The analytical solutions of incompressible saturated poroelastic circular Mindlin's plate", *J. Appl. Mech.*, **79**(5), 203-210.

Whitney, J. (1972), "Stress analysis of thick laminated composite and sandwich plates", *J. Compos. Mater.*, **6**, 426-440.

Yahia, S.A., Atmane, H.A., Houari, M.S.A. and Tounsi, A. (2015), "Wave propagation in functionally graded plates with porosities using various higher-order shear deformation plate theories", *Struct. Eng. Mech., Int. J.*, **53**(6), 1143-1165.

Yin, L., Qian, Q., Wang, L. and Xia, W. (2010), "Vibration analysis of micro scale plates based on modified couple stress theory", *Acta Mech. Solid Sin.*, **23**, 386-393.

Zeighampour, H. and Beni, Y.T. (2014), "Cylindrical thin-shell model based on modified strain gradient theory", *Int. J. Eng. Sci.*, **78**, 27-47.

Zemri, A., Houari, M.S.A., Bousahla, A.A. and Tounsi, A. (2015), "A mechanical response of functionally graded nanoscale beam: an assessment of a refined nonlocal shear deformation theory beam theory", *Struct. Eng. Mech., Int. J.*, **54**(4), 693-710.

Zenkour, A. (2005), "A comprehensive analysis of functionally graded sandwich plates, Part 1 - deflection and stresses", *Int. J. Solids Str.*, **42**, 5224-5242.

Zhao, C. (2012), "Review on thermal transport in high porosity cellular metal foams with open cells", *Int. J. Heat Mass Transf.*, **55**, 3618-3632.

Zhang, L.W. (2017a), "Geometrically nonlinear large deformation of CNT-reinforced composite plates with internal column supports", *J. Model. Mech. Mater.*, **1**, 20160154. DOI: https://doi.org/10.1515/nano.0070.00001

Zhang, L.W. (2017b), "On the study of the effect of in-plane forces on the frequency parameters of CNT-reinforced composite skew plates", *Compos. Struct.*, **160**, 824-837.

Zhang, L.W. and Liew, K.M. (2016a), "Postbuckling analysis of axially compressed CNT reinforced functionally graded composite plates resting on Pasternak foundations using an element-free approach", *Compos. Struct.*, **138**, 40-51.

Zhang, L.W. and Liew, K.M. (2016b), "Element-free geometrically nonlinear analysis of quadrilateral functionally graded material plates with internal column supports", *Compos. Struct.*, **147**, 99-110.

Zhang, L.W. and Selim, B.A. (2017), "Vibration analysis of CNT-reinforced thirck laminated composite plates based on Reddy's higher-order shear deformation theory", *Compos. Struct.*, **160**, 689-705.

Zhang, L.W. and Xiao, L.N. (2017), "Mechanical behavior of laminated CNT-reinforced composite skew plates subjected to dynamic loading", *Compos. part B*, **122**, 219-230.

Zhang, L.W. and Liew, K.M. (2015), "Large deflection analysis of FG-CNT reinforced composite skew plates resting on Pasternak foundations using an element-free approach", *Compos. Struct.*, **132**, 974-993.

Zhang, L.W., Zhub, P. and Liew, K.M. (2014), "Thermal buckling of functionally graded plates using a local Kriging meshless method", *Compos. Struct.*, **108**, 472-492**.**

Zhang, L.W., Huang, D. and Liew, K.M. (2015a), "An element-free IMLS-Ritz method for numerical solution of three-dimensional wave equations", *Comput. Meth. Appl. Mech. Eng.*, **297**, 116-139.

Zhang, L.W., Song, Z.G. and Liew, K.M. (2015b), "State-space Levy method for vibration analysis of FG-CNT composite plates subjected to in-plane loads based on higher-order shear deformation theory", *Compos. Struct.*, **134**, 989-1003.

Zhang, L.W., Song, Z.G. and Liew, K.M. (2015c), "Nonlinear bending analysis of FG-CNT reinforced composite thick plates resting on Pasternak foundations using the element-free IMLS-Ritz method", *Compos. Struct.*, **128**, 165-175.

Zhang, L.W., Lei, Z.X. and Liew, K.M. (2015d), "Buckling analysis of FG-CNT reinforced composite thick skew plates using an element-free approach", *Compos. part B*, **75**, 36-46.

Zhang, L.W., Liew, K.M. and Jiang, Z. (2016a), "An element-free analysis of CNT-reinforced composite plates with column supports and elastically restrained edges under large deformation", *Compos. part B*, **95**, 18-28.

Zhang, L.W., Liew, K.M. and Reddy, J.N. (2016b), "Postbuckling of carbon nanotube reinforced functionally graded plates with edges elastically restrained against translation and rotation under axial compression", *Comput. Meth. Appl. Mech. Eng.*, **298**, 1-28.

Zhang, L.W., Xiao, L.N., Zou, G.L. and Liew , K.M. (2016c), "Elastodynamic analysis of quadrilateral CNT-reinforced functionally graded composite plates using FSDT element-free method", *Compos. Struct.*, **148**, 144-154.

Zhang, L.W., Zhang, Y., Zou, G.L. and Liew, K.M. (2016d), "Free vibration analysis of triangular CNT-reinforced composite plates subjected to in-plane stresses using FSDT element-free method", *Compos. Struct.*, **149**, 247-260.

Zhang, L.W., Liew, K.M. and Reddy, J.N. (2016e), "Postbuckling analysis of bi-axially compressed laminated nanocomposite plates using the first-order shear deformation theory", *Compos. Struct.*, **152**, 418-431.

Zhang, L.W., Song, Z.G. and Liew, K.M. (2016f), "Optimal shape control of CNT reinforced functionally graded composite plates using piezoelectric patches", *Compos. part B*, **85**, 140-149.

Zhang, L.W., Song, Z.G. and Liew, K.M. (2016g), "Computation of aerothermoelastic properties and active flutter control of CNT reinforced functionally graded composite panels in supersonic airflow", *Comput. Meth. Appl. Mech. Eng.*, **300**, 427-441.

Zhang, L.W., Liu, W.H. and Liew, K.M. (2016h), "Geometrically nonlinear large deformation analysis of triangular CNT-reinforced composite plates", *Int. J. Non-Linear Mech.*, **86**, 122-132.

Zhong, R., Wang, Q., Tang, J., Shuai, C. and Qin, B. (2018), "Vibration analysis of functionally graded carbon nanotube reinforced composites (FG-CNTRC) circular, annular and sector plates", *Compos. Struct.*, **194**(15), 49-67.

Zhou, D., Au, F.T.K., Cheung, Y.K. and Lo, S.H. (2003), "Three-dimensional vibration analysis of circular and annular plates via the Chebyshev–Ritz method", *Int. J. Solids Struct.*, **40**, 3089-3105.

Zhu, P., Zhang, L.W. and Liew, K.M. (2014), "Geometrically nonlinear thermo mechanical analysis of moderately thick functionally graded plates using a local Petrov–Galerkin approach with moving Kriging interpolation", *Compos. Struct.*, **107**, 298-314.

CC